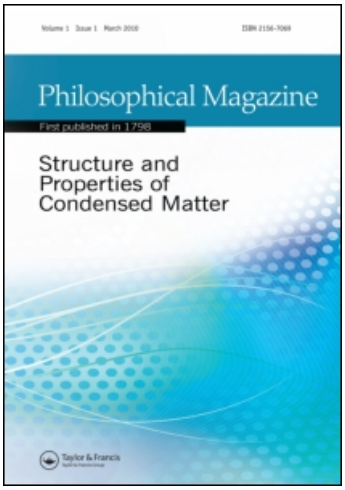

Philosophical Magazine
Publication details, including instructions for authors and subscription information:
http://www.informaworld.com/smpp/title~content=t713695589

Dilatational viscoplasticity of polycrystalline solids with intergranular cavities

R. A. Lebensohn[a]; M. I. Idiart[bc]; P. Ponte Castañeda[de]; P. -G. Vincent[fg]
[a] Materials Science and Technology Division, Los Alamos National Laboratory, Los Alamos, NM 87545, USA [b] Departamento de Aeronáutica, Facultad de Ingeniería, Universidad Nacional de La Plata, La Plata B1900TAG, Argentina [c] Consejo Nacional de Investigaciones Científicas y Técnicas (CONICET), de Buenos Aires C1033AAJ, Argentina [d] Department of Mechanical Engineering and Applied Mechanics, University of Pennsylvania, Philadelphia, PA 19104-6315, USA [e] Madrid Institute for Advanced Studies of Materials, Madrid, E-28040, Spain [f] Laboratoire de Mécanique et d'Acoustique/CNRS, 13402 Marseille, France [g] Institut de Radioprotection et de Sûreté Nucléaire (IRSN), 13115 Saint-Paul-Lez-Durance Cedex, France

First published on: 05 April 2011

To cite this Article Lebensohn, R. A. , Idiart, M. I. , Castañeda, P. Ponte and Vincent, P. -G.(2011) 'Dilatational viscoplasticity of polycrystalline solids with intergranular cavities', Philosophical Magazine,, First published on: 05 April 2011 (iFirst)
To link to this Article: DOI: 10.1080/14786435.2011.561811
URL: http://dx.doi.org/10.1080/14786435.2011.561811

Philosophical Magazine
2011, 1–30, iFirst

Taylor & Francis
Taylor & Francis Group

Dilatational viscoplasticity of polycrystalline solids with intergranular cavities

R.A. Lebensohn[a]*, M.I. Idiart[bc], P. Ponte Castañeda[de] and P.-G. Vincent[fg]

[a]Materials Science and Technology Division, Los Alamos National Laboratory, MS G755, Los Alamos, NM 87545, USA; [b]Departamento de Aeronáutica, Facultad de Ingeniería, Universidad Nacional de La Plata, Calles 1 y 47, La Plata B1900TAG, Argentina; [c]Consejo Nacional de Investigaciones Científicas y Técnicas (CONICET), Avda. Rivadavia 1917, Cdad. de Buenos Aires C1033AAJ, Argentina; [d]Department of Mechanical Engineering and Applied Mechanics, University of Pennsylvania, Philadelphia, PA 19104-6315, USA; [e]Madrid Institute for Advanced Studies of Materials, Madrid, E-28040, Spain; [f]Laboratoire de Mécanique et d'Acoustique/CNRS, 31 Chemin Joseph Aiguier, 13402 Marseille, France; [g]Institut de Radioprotection et de Súreté Nucléaire (IRSN), DPAM, BP3, 13115 Saint-Paul-Lez-Durance Cedex, France

(*Received 27 August 2010; final version received 5 February 2011*)

We propose constitutive models for polycrystalline aggregates with intergranular cavities and test them against full-field numerical simulations. Such conditions are prevalent in many engineering applications and failure of metallic components (e.g. HIPing and other forming processes, spallation under dynamic loading conditions, etc.), where the dilatational effects associated with the presence of cavities must be accounted for, and standard polycrystalline models for incompressible plasticity are not appropriate. On the other hand, it is not clear that the use of porous plasticity models with isotropic matrix behavior is relevant, particularly, when large deformations can lead to significant texture evolution and therefore to strong matrix anisotropy. Of course, finite strains can also lead to significant changes in the porosity and pore shape, resulting in additional anisotropy development. In this work, we make use of 'variational linear-comparison' homogenization methods to develop constitutive models simultaneously accounting for texture of the matrix, porosity and average pore shape and orientation. The predictions of the models are compared with full-field numerical simulations based on fast Fourier transforms to study the influence of different microstructural features (e.g. overall porosity, texture of the matrix phase, single-crystal anisotropy, etc.) and type of loading (triaxiality) on the dilatational viscoplastic behavior of voided polycrystals. The results are also compared with the predictions of isotropic-matrix porous plasticity models to assess the effect of the possible matrix anisotropy in textured samples.

Keywords: voids; plasticity of metals; texture; anisotropic properties

*Corresponding author. Email: lebenso@lanl.gov

ISSN 1478–6435 print/ISSN 1478–6443 online

DOI: 10.1080/14786435.2011.561811
http://www.informaworld.com

1. Introduction

The aim of this work is to provide constitutive models for the viscoplastic response of polycrystalline aggregates accounting for the dilatational effects associated with the presence of intergranular cavities. These conditions are prevalent in many engineering problems (e.g. HIPing and other forming processes) where the dilatational effects associated with the presence of cavities must be accounted for, and standard polycrystalline models for incompressible plasticity are not appropriate.

A particularly important problem that calls for such constitutive models is the ductile failure of metals and other polycrystalline solids by void growth to coalescence [1,2]. Experimental observations on rolled [1,3,4] and extruded [5] engineering alloys show that crystallographic and morphological textures can induce strongly anisotropic damage growth and fracture behavior. Texture has also been found to result in anisotropic spallation of low-symmetry metals under shock loading [6,7]. Most available theories of dilatational viscoplasticity, however, make use of the simplifying assumption that the matrix material is homogeneous and isotropic, and are therefore unable to capture texture effects. This is the case, for instance, of the celebrated theory of Gurson [8] and its various generalizations proposed by Leblond et al. [9], Gologanu et al. [10], and Gărăjeu et al. [11], among others. These theories are collectively referred to as Gurson-type theories, and are all based on approximate solutions of an isotropic hollow sphere subject to axisymmetric loadings. Recent work by Benzerga et al. [12], Monchiet et al. [13], Keralavarma and Benzerga [14] and others have explored ways to incorporate plastic anisotropy into these models by assuming that the plastic matrix obeys an anisotropic yield criterion of the form proposed by Hill [15]. However, this approach is restricted to rate-independent plasticity with orthotropic yield criteria, and, in principle, cannot account for the evolution of plastic anisotropy due to deformation-induced changes in texture. In contrast, the dilatational viscoplasticity theories for polycrystalline voided solids will be derived in this work by generalizing *polycrystal models*, accounting for the heterogeneity associated with both the crystallites and the cavities on an equal footing.

Several constitutive theories are already available to estimate the viscoplastic response of *fully dense* polycrystalline solids in terms of their morphological and crystallographic texture. For *linearly* viscous polycrystals, the so-called *self-consistent* theory has been found to be both very accurate [16,17] and easy-to-use. This linear theory was originally proposed – in the mathematically analogous context of elasticity – as an *ad hoc* model consisting in the use of the Eshelby solution to approximate the grain interactions through the replacement of all other grains by an effective medium – chosen in a self-consistent manner – by Hershey [18] and Kröner [19], and was later derived more rigorously via the Hashin–Shtrikman variational principles [20], and endowed with a clear statistical interpretation, by Willis [21]. Driven by the need to understand plastic deformation in metals and other polycrystalline solids, many attempts have been made to generalize the self-consistent theory to *nonlinear* constitutive responses.

Among the earlier nonlinear self-consistent theories, perhaps the most popular are the 'incremental' theory of Hill [22] and Hutchinson [23], and the 'tangent' procedure of Molinari et al. [24] and Lebensohn and Tomé [25]. These theories – and

their various variants – also made use of the linear Eshelby solution, together with an appropriately chosen linearization scheme to approximate the grain interactions. However, while the 'incremental' and 'tangent' theories generally provide improvements on the elementary Taylor and Sachs approximations, they can give inaccurate predictions for low rate-sensitivity materials, especially when crystal anisotropy is large. And even more importantly for our purposes, these classical theories are already known to give unphysical predictions for isotropic voided solids [26], the reason being that their linearization schemes are based on the first moments of the fields only, while the presence of cavities induces strong field gradients in the solid phases, making it necessary to use linearization schemes that should also incorporate higher-order information on the field distributions.

A new class of nonlinear self-consistent theories, improving considerably on the above 'classical' theories, is available from the work of Ponte Castañeda and co-workers. These theories rely on the use of a 'linear-comparison polycrystal' (LCP), consisting of a polycrystal with the same microstructure as the nonlinear polycrystal but whose single-crystal response is identified with a certain linearization of the corresponding nonlinear response, typically guided by suitably designed variational principles. Then, the standard (linear) self-consistent theory can be used to estimate the macroscopic response of the linear-comparison polycrystal, which in turn can be used to estimate the macroscopic response of the nonlinear polycrystal. The difference between the various 'linear-comparison' theories proposed in the literature lies on the choice of the linearization scheme. The first 'linear-comparison' variational estimates of the self-consistent type for viscoplastic polycrystals were derived by Ponte Castañeda and Nebozhyn [27], making use of the variational approach of deBotton and Ponte Castañeda [28] and building on earlier work by Ponte Castañeda [29] for isotropic nonlinear materials. This theory uses a secant approximation to the nonlinear local response evaluated at the second moments of the fields [30,31], and yields rigorous bounds for all other self-consistent theories. This fact was used to demonstrate the inconsistency of the 'incremental' theory, which was often found to violate those bounds [32]. A refined version of the 'secant' variational theory has been recently derived by Idiart and Ponte Castañeda [33], which can deliver sharper bounds [34] at the expense of introducing a more complicated optimization problem. However, precisely because of their bounding property, the 'secant' variational estimates are expected to be rather stiff. Softer estimates were derived by Bornert et al. [35], making use of a linear-comparison procedure proposed by Ponte Castañeda [36] and endowed with a variational status by Ponte Castañeda and Willis [37]. This procedure uses a tangent approximation to the nonlinear local response evaluated at the first moments of the fields, and generates estimates that are exact to second-order in the heterogeneity contrast. A simplified version of this procedure, referred to as the 'affine' procedure, is available from the work of Masson et al. [26]. However, precisely because the linearization scheme is based on first moments only, these 'tangent' variational estimates give poor predictions for extremely heterogeneous systems. For isotropic voided solids in particular, they predict non-convex stress potentials with unbounded hydrostatic strength [38,39]. More recently, Liu and Ponte Castañeda [40], building on earlier work by Ponte Castañeda [41], proposed an improved 'second-order' theory that makes use of a 'generalized-secant' interpolation of the nonlinear local response,

incorporating dependence on both the first and second moments of the fields, while at the same time, preserving the exactness to second-order in the contrast. Comparisons with full-field numerical simulations for cubic and hexagonal polycrystals show that the generalized-secant variational theory is the most accurate among the various nonlinear self-consistent theories available to date [16,17,42,43].

Even though all theories mentioned above can be extended to account for a vacuous phase, their use in the context of polycrystalline *voided* solids remains largely unexplored, presumably because of the additional complications introduced by the presence of a compressible phase. The use of an incremental theory was first attempted by Lebensohn et al. [4] to model anisotropic damage in aluminum alloys. This work was restricted to small-strain elastoplasticity. More recently, Lebensohn et al. [44] made use of the affine procedure to model the viscoplastic response of voided polycrystals. In order to achieve reasonable accuracy, however, these authors introduced a modified linearization scheme to soften the response at high porosities and triaxialities, which requires the numerical computation of a fitting parameter that depends on loading, porosity, and material properties.

Motivated by these findings, dilatational viscoplasticity models for polycrystalline voided solids will be derived in this work by extending the generalized-secant variational theory. The resulting models will be general enough to account for (i) morphological and crystallographic texture of the polycrystalline matrix, (ii) porosity, and (iii) average pore shape and orientation, as well as their deformation-induced evolution under arbitrary loading conditions. Even though such a degree of generality will prevent us from obtaining analytical closed-form expressions as in the case of Gurson-type approaches, the models should be amenable to implementation in dynamic finite-element codes. In order to assess their accuracy, bounds are derived by extending the simpler 'secant' variational theory.

The models are also validated by comparing their predictions with full-field numerical simulations for voided polycrystals. In the context of isotropic voided solids, full-field simulations have been carried out mostly by means of Finite Element (FE) methods. In the present context, such FE calculations would require the use of 3-D crystal-plasticity (CP) with high intragranular resolution and a sufficient number of grains to guarantee a good statistical representativity of the results. With these requirements, the implementation of such 3-D CP-FE calculations becomes a daunting task. Alternatively, in this work we perform the required reference full-field numerical simulations by means of a fast Fourier transform (FFT)-based method. This method, which provides the exact solution of the governing equations in a periodic medium, has better numerical performance than a FE calculation for the same purpose and resolution. It was originally developed by Suquet and co-workers [45–47] as a fast algorithm to compute the elastic and elastoplastic effective and local response of composites, and was later adapted by Lebensohn and co-workers [17,43,48] to deal with the viscoplastic deformation of three-dimensional (3-D) power-law polycrystals. The full-field simulations and various models are then used to investigate the effect of crystallinity, crystallographic texture and porosity in polycrystalline solids with low- and high-symmetry crystals. Also, the validity of standard dilatational viscoplasticity models based on isotropic matrix behavior is evaluated for various types of textured and untextured polycrystals.

2. The polycrystalline solid model

Voided polycrystals are idealized here as random aggregates of perfectly bonded single crystals (i.e. grains) and cavities. Individual grains and cavities are assumed to be of a similar size, much smaller than the specimen size and the scale of variation of the applied loads. Furthermore, the aggregates are assumed to have statistically uniform and ergodic microstructures. Their viscoplastic behavior is most conveniently studied by adopting a Eulerian description of motion. The ensuing analysis thus refers to the *current* configuration of the aggregate at a generic stage of deformation.

Let the grain orientations in the current configuration take on a set of N discrete values, characterized by rotation tensors $\mathbf{Q}^{(r)}$ $(r=1,\ldots,N)$. All grains with a given orientation $\mathbf{Q}^{(r)}$ occupy a disconnected domain $\Omega^{(r)}$ and are collectively referred to as 'phase' r. Similarly, all cavities occupy a disconnected domain $\Omega^{(0)}$ and are collectively referred to as 'phase' 0. The domain occupied by the polycrystal is then $\Omega=\cup_{r=0}^{N}\Omega^{(r)}$. The domains $\Omega^{(r)}$ can be described by a set of characteristic functions $\chi^{(r)}(\mathbf{x})$, which take the value 1 if the position vector $\mathbf{x}$ is in $\Omega^{(r)}$ and 0 otherwise.

Grains are assumed to individually deform by multi-glide along K slip systems. Cavities, on the other hand, cannot sustain stress. The effects of grain elasticity and possible twinning will be neglected in this work, for simplicity. The local viscoplastic response of the aggregate can then be described by a stress potential u, such that the Eulerian strain-rate tensor $\boldsymbol{D}$ and the stress tensor $\boldsymbol{\sigma}$ are related by

$$\boldsymbol{D}=\frac{\partial u}{\partial \boldsymbol{\sigma}}(\mathbf{x},\boldsymbol{\sigma}),\quad u(\mathbf{x},\boldsymbol{\sigma})=\sum_{r=0}^{N}\chi^{(r)}(\mathbf{x})u^{(r)}(\boldsymbol{\sigma}). \tag{1}$$

Here, $u^{(0)}$ is the stress potential for the voided phase, which takes the value 0 if $\boldsymbol{\sigma}=\mathbf{0}$ and infinity otherwise, and $u^{(1)},\ldots,u^{(N)}$ are the stress potentials characterizing grains with orientation $\mathbf{Q}^{(1)},\ldots,\mathbf{Q}^{(N)}$, given by

$$u^{(r)}(\boldsymbol{\sigma})=\sum_{k=1}^{K}\phi_{(k)}^{(r)}\left(\tau_{(k)}^{(r)}\right). \tag{2}$$

The convex functions $\phi_{(k)}^{(r)}$ $(k=1,\ldots,K)$ characterize the response of the K slip systems in a crystal with orientation $\mathbf{Q}^{(r)}$, and depend on the resolved shear (or Schmid) stresses

$$\tau_{(k)}^{(r)}=\boldsymbol{\sigma}\cdot\boldsymbol{\mu}_{(k)}^{(r)},\quad \text{where } \boldsymbol{\mu}_{(k)}^{(r)}=\frac{1}{2}\left(\mathbf{n}_{(k)}^{(r)}\otimes\mathbf{m}_{(k)}^{(r)}+\mathbf{m}_{(k)}^{(r)}\otimes\mathbf{n}_{(k)}^{(r)}\right). \tag{3}$$

Here, the $\boldsymbol{\mu}_{(k)}^{(r)}$ are second-order tensors with $\mathbf{n}_{(k)}^{(r)}$ and $\mathbf{m}_{(k)}^{(r)}$ denoting the unit vectors normal to the slip plane and along the slip direction of the kth system, respectively, for a crystal with orientation $\mathbf{Q}^{(r)}$. Note that the Schmid tensors $\boldsymbol{\mu}_{(k)}^{(r)}$ are related to corresponding tensors $\boldsymbol{\mu}_{(k)}$ for a 'reference' crystal via $\boldsymbol{\mu}_{(k)}^{(r)}=\mathbf{Q}^{(r)^{T}}\boldsymbol{\mu}_{(k)}\mathbf{Q}^{(r)}$.

Let $\langle\cdot\rangle$ and $\langle\cdot\rangle^{(r)}$ denote volume averages over the aggregate Ω and over each phase $\Omega^{(r)}$, respectively. In view of the microstructural randomness, the functions $\chi^{(r)}$ in (1) are random variables that must be characterized in terms of ensemble averages [21]. The ensemble average of $\chi^{(r)}(\mathbf{x})$ represents the one-point probability $p^{(r)}(\mathbf{x})$ of

finding phase r at $\mathbf{x}$; the ensemble average of the product $\chi^{(r)}(\mathbf{x})\chi^{(s)}(\mathbf{x}')$ represents the two-point probabilities $p^{(rs)}(\mathbf{x}, \mathbf{x}')$ of finding simultaneously phase r at $\mathbf{x}$ and phase s at $\mathbf{x}'$. Higher-order probabilities are defined similarly. Due to the assumed statistical uniformity and ergodicity, the one-point probability $p^{(r)}(\mathbf{x})$ can be identified with the volume fractions – or concentrations – $c^{(r)} = \langle \chi^{(r)}(\mathbf{x}) \rangle$ of each phase r, the two-point probability $p^{(rs)}(\mathbf{x}, \mathbf{x}')$ can be identified with the volume average $\langle \chi^{(r)}(\mathbf{x})\chi^{(s)}(\mathbf{x}') \rangle$, and so on. Note that $\sum_{r=0}^{N} c^{(r)} = 1$. In describing voided polycrystals, it seems more natural to employ the alternative set of concentrations:

$$f = c^{(0)}, \quad \text{and} \quad c_g^{(r)} = \frac{c^{(r)}}{1-f} \quad \text{for } r = 1, \ldots, N. \tag{4}$$

The microstructural variable f denotes the volume fraction of cavities, or *porosity*, in the voided polycrystal, while the rescaled grain concentrations $c_g^{(r)}$ denote the volume fraction of grains with a given orientation $\mathbf{Q}^{(r)}$ within the solid phase, and are such that $\sum_{r=1}^{N} c_g^{(r)} = 1$. Thus, the set of volume fractions $c_g^{(r)}$ characterizes the *crystallographic texture* of the aggregate surrounding the cavities, while the multi-point correlation functions characterize the *morphological texture* of the aggregate and the shape and distribution of the cavities.

Due to the microstructural inhomogeneity, the local fields $\boldsymbol{D}(\mathbf{x})$ and $\boldsymbol{\sigma}(\mathbf{x})$ exhibit strong spatial variations within the aggregate. The effective viscoplastic behavior of the aggregate is defined as the relation between the average stress $\overline{\boldsymbol{\sigma}} = \langle \boldsymbol{\sigma} \rangle$ and the average strain rate $\overline{\boldsymbol{D}} = \langle \boldsymbol{D} \rangle$ over the aggregate. Formally, it can be characterized by (e.g. [31])

$$\overline{\boldsymbol{D}} = \frac{\partial \widetilde{u}}{\partial \overline{\boldsymbol{\sigma}}}(\overline{\boldsymbol{\sigma}}), \quad \widetilde{u}(\overline{\boldsymbol{\sigma}}) = \min_{\boldsymbol{\sigma} \in \mathcal{S}(\overline{\boldsymbol{\sigma}})} \langle u(\mathbf{x}, \boldsymbol{\sigma}) \rangle = (1-f) \min_{\boldsymbol{\sigma} \in \mathcal{S}^*(\overline{\boldsymbol{\sigma}})} \sum_{r=1}^{N} c_g^{(r)} \langle u^{(r)}(\boldsymbol{\sigma}) \rangle^{(r)}, \tag{5}$$

where $\widetilde{u}$ is the *effective stress potential* for the aggregate. In this definition, $\mathcal{S}(\overline{\boldsymbol{\sigma}}) = \{\boldsymbol{\sigma} | \operatorname{div} \boldsymbol{\sigma} = \mathbf{0} \text{ in } \Omega, \langle \boldsymbol{\sigma} \rangle = \overline{\boldsymbol{\sigma}}\}$ denotes the set of statically admissible stress fields with prescribed average $\overline{\boldsymbol{\sigma}}$, while $\mathcal{S}^* \subset \mathcal{S}$ denotes the subset of stress fields with zero traction vector on the surface of the cavities. The (strict) convexity of the local potential u in $\boldsymbol{\sigma}$ implies (strict) convexity of the effective potential $\widetilde{u}$ in $\overline{\boldsymbol{\sigma}}$. The minimizer in $(5)_2$ corresponds to the stress field within the aggregate under the prescribed loading conditions. Carrying out this minimization is in general a formidable task, since it requires the solution to sets of nonlinear partial differential equations with randomly oscillatory coefficients. In Section 3, we will generate approximate *estimates* for the effective potential by means of variational 'linear-comparison' methods. Corresponding estimates for the effective behavior of the aggregate may then be generated by differentiation, according to relation $(5)_1$. This relation provides the *instantaneous* response of the aggregate. A continuing process of deformation can then be analyzed by integrating over time the instantaneous response along with appropriate evolution laws for the internal variables characterizing the underlying texture and porosity [49]. Such laws require statistical information about the strain-rate distribution within the solid, which can also be extracted from the effective potential [50]. In this work, however, we will focus exclusively on the estimation of the instantaneous response.

3. Estimates of the self-consistent type for the effective stress potential

Estimates and bounds for the effective stress potential of voided polycrystals are generated here by means of the linear-comparison variational theories of Liu and Ponte Castañeda [40] and deBotton and Ponte Castañeda [28], which will be referred to as 'generalized secant' and 'secant,' respectively. (The latter use should not be confused with more traditional usages [23].) When used in conjunction with the linear self-consistent theory, these nonlinear estimates incorporate microstructural information up to two-point statistics. We begin by recalling the relevant formulas for the linear self-consistent theory.

3.1. *Linear self-consistent estimates*

The nonlinear theories considered in this work make use of a 'thermoelastic' linear-comparison voided polycrystal (or more precisely, a porous linearly viscous polycrystal with prescribed internal strain rates) with local stress–strain-rate relations of the form $\boldsymbol{D} = \mathbf{M}^{(r)}\boldsymbol{\sigma} + \mathbf{e}^{(r)}$, where $\mathbf{M}^{(r)}$ and $\mathbf{e}^{(r)}$ are viscous-compliance and 'residual' strain-rate tensors in each phase r, respectively – see Figure 1 below. For the voided phase, $(\mathbf{M}^{(0)})^{-1} = \mathbf{0}$ and $\mathbf{e}^{(0)} = \mathbf{0}$. The associated stress potentials can be written as

$$u_L^{(r)}(\boldsymbol{\sigma}) = \frac{1}{2}\boldsymbol{\sigma} \cdot \mathbf{M}^{(r)}\boldsymbol{\sigma} + \mathbf{e}^{(r)} \cdot \boldsymbol{\sigma}, \tag{6}$$

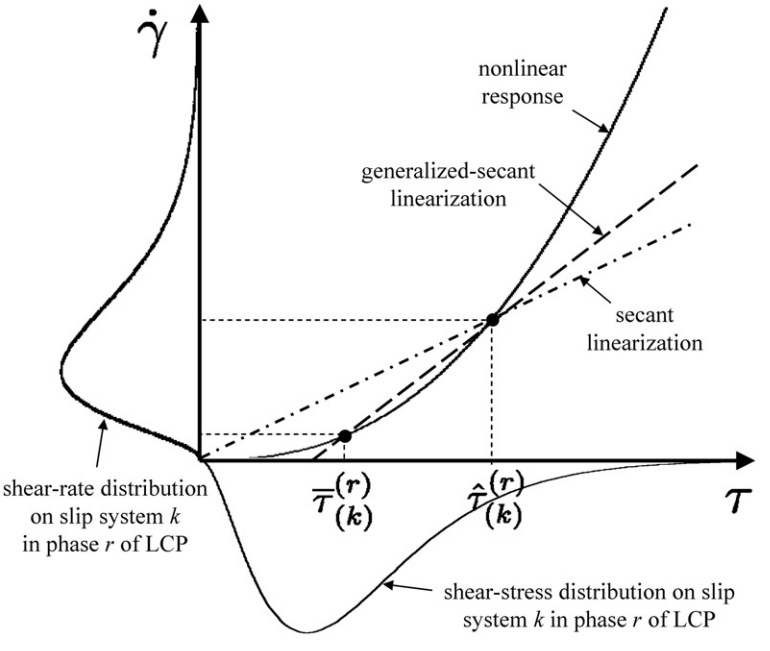

Figure 1. 'Generalized-secant' and 'secant' linearization schemes.

and the corresponding effective stress potential is given by

$$\widetilde{u}_L(\overline{\boldsymbol{\sigma}}) = (1-f)\min_{\boldsymbol{\sigma}\in\mathcal{S}^*(\overline{\boldsymbol{\sigma}})}\sum_{r=1}^{N} c_g^{(r)}\langle u_L^{(r)}(\boldsymbol{\sigma})\rangle^{(r)}. \tag{7}$$

A subscript L is used here to identify potentials associated with linear polycrystals.

Self-consistent estimates for thermoelastic systems are available from the work of Laws [51] and Willis [52]. When the local stress potentials are of the form (6) and one of the phases is vacuous, the effective stress potential (7) may be written in the form

$$\widetilde{u}_L(\overline{\boldsymbol{\sigma}}) = \frac{1}{2}\overline{\boldsymbol{\sigma}}\cdot\widetilde{\mathbf{M}}\overline{\boldsymbol{\sigma}} + \widetilde{\mathbf{e}}\cdot\overline{\boldsymbol{\sigma}} + \frac{1}{2}\widetilde{g}, \tag{8}$$

where the overall properties can be shown to reduce to

$$\begin{aligned}
\widetilde{\mathbf{M}} &= \sum_{r=1}^{N} c_g^{(r)}\mathbf{M}^{(r)}\mathbf{B}^{(r)} + \frac{f}{1-f}\widetilde{\mathbf{M}}^*,\\
\widetilde{\mathbf{e}} &= (1-f)\sum_{r=1}^{N} c_g^{(r)}\mathbf{B}^{(r)^T}\mathbf{e}^{(r)}, \quad \text{and}\\
\widetilde{g} &= (1-f)\sum_{r=1}^{N} c_g^{(r)}\mathbf{b}^{(r)}\cdot\mathbf{e}^{(r)}
\end{aligned} \tag{9}$$

which are the effective viscous compliance, effective residual strain rate and effective energy under zero applied stress, respectively. In these expressions, $\mathbf{B}^{(r)}$ and $\mathbf{b}^{(r)}$ are concentration tensors given by

$$\mathbf{B}^{(r)} = \left(\mathbf{M}^{(r)} + \widetilde{\mathbf{M}}^*\right)^{-1}\left(\widetilde{\mathbf{M}} + \widetilde{\mathbf{M}}^*\right) \quad \text{and} \quad \mathbf{b}^{(r)} = \left(\mathbf{M}^{(r)} + \widetilde{\mathbf{M}}^*\right)^{-1}\left(\widetilde{\mathbf{e}} - \mathbf{e}^{(r)}\right), \tag{10}$$

$\widetilde{\mathbf{M}}^* = \widetilde{\mathbf{Q}}^{-1} - \widetilde{\mathbf{M}}$ is the constraint tensor introduced by Hill [22], and $\widetilde{\mathbf{Q}}$ is a microstructural tensor that depends on $\widetilde{\mathbf{M}}$ and on the 'shape' of the two-point correlation functions $p^{(rs)}(\mathbf{x},\mathbf{x}')$ for the distribution of the grain orientations and the porosity within the aggregate. In this work, it is assumed that the two-point correlation functions exhibit 'ellipsoidal symmetry', that is: $p^{(rs)}(\mathbf{x},\mathbf{x}') = p(|\mathbf{Z}(\mathbf{x}-\mathbf{x}')|)$ for all r and s, where $\mathbf{Z}$ is a symmetric second-order tensor serving to characterize the 'shape' of the distribution. In particular, $\mathbf{Z}=\mathbf{I}$ corresponds to the special case of statistical isotropy, which is equivalent to the so-called 'equi-axed' hypothesis. More generally, the tensor $\mathbf{Z}$ allows for changes in the average shape of grains and cavities when the polycrystal is subjected to finite deformation histories. Under the assumption of ellipsoidal symmetry, the tensor $\widetilde{\mathbf{Q}}$ may be expressed in terms of the effective viscous moduli tensor $\widetilde{\mathbf{L}} = \widetilde{\mathbf{M}}^{-1}$ and a microstructural tensor $\widetilde{\mathbf{P}}$ as $\widetilde{\mathbf{Q}} = \widetilde{\mathbf{L}} - \widetilde{\mathbf{L}}\widetilde{\mathbf{P}}\widetilde{\mathbf{L}}$, where [21]

$$\widetilde{\mathbf{P}} = \frac{1}{4\pi\det\mathbf{Z}}\int_{|\boldsymbol{\xi}|=1}\widetilde{\mathbf{H}}(\boldsymbol{\xi})|\mathbf{Z}^{-1}\boldsymbol{\xi}|^{-3}\,\mathrm{d}S. \tag{11}$$

Here, $\widetilde{H}_{ijkl}(\boldsymbol{\xi}) = \widetilde{K}_{ik}^{-1}\xi_j\xi_l\,|_{(ij)(kl)}$ and $\widetilde{K}_{ik} = \widetilde{L}_{ijkl}\xi_j\xi_l$. Note that in this model, cavities and grains are treated on the same footing, which corresponds to the problem of a polycrystal with *inter*granular cavities. This is in contrast to aggregates of grains

exhibiting *intra*granular porosity, which should be treated differently, using, for instance, a three-scale approach [53].

Finally, $\widetilde{\mathbf{M}}$ solves the implicit equation

$$\left(\widetilde{\mathbf{M}}+\widetilde{\mathbf{M}}^{*}\right)^{-1}=(1-f)\sum_{r=1}^{N}c_{g}^{(r)}\left(\mathbf{M}^{(r)}+\widetilde{\mathbf{M}}^{*}\right)^{-1}, \tag{12}$$

which follows from the combination of expressions $(10)_1$ and $(10)_2$.

The associated estimate for the effective stress–strain-rate relation follows from differentiation of (8), and is given by

$$\overline{\boldsymbol{D}}=\widetilde{\mathbf{M}}\overline{\boldsymbol{\sigma}}+\widetilde{\mathbf{e}}. \tag{13}$$

In turn, corresponding estimates for the first and second moments of the stress field in each solid phase r, which are required by the linear-comparison theories below, are given by

$$\overline{\boldsymbol{\sigma}}^{(r)}=\mathbf{B}^{(r)}\overline{\boldsymbol{\sigma}}+\mathbf{b}^{(r)}\quad\text{and}\quad\langle\boldsymbol{\sigma}\otimes\boldsymbol{\sigma}\rangle^{(r)}=\frac{1}{1-f}\frac{2}{c_{g}^{(r)}}\frac{\partial\widetilde{u}_{L}}{\partial\mathbf{M}^{(r)}}. \tag{14}$$

The second moments of the intraphase stress fluctuations then follow from the identity

$$\mathbf{C}_{\boldsymbol{\sigma}}^{(r)}=\left\langle(\boldsymbol{\sigma}-\overline{\boldsymbol{\sigma}}^{(r)})\otimes(\boldsymbol{\sigma}-\overline{\boldsymbol{\sigma}}^{(r)})\right\rangle^{(r)}=\langle\boldsymbol{\sigma}\otimes\boldsymbol{\sigma}\rangle^{(r)}-\overline{\boldsymbol{\sigma}}^{(r)}\otimes\overline{\boldsymbol{\sigma}}^{(r)}. \tag{15}$$

3.2. *Nonlinear 'generalized-secant' estimates*

Estimates for the effective potential of nonlinear voided polycrystals are generated here by means of the 'generalized-secant' variational theory of Liu and Ponte Castañeda [40]. This second-order theory was originally derived for the case of fully dense polycrystals under the assumption of incompressible constituent phases. In this section we extend the theory to account for the presence of a compressible voided phase.

The theory makes use of a linear-comparison voided polycrystal with the same microstructure as the nonlinear polycrystal but with local stress potentials $u^{(r)}$ given by (6), where

$$\mathbf{M}^{(r)}=\sum_{k=1}^{K}\alpha_{(k)}^{(r)}\boldsymbol{\mu}_{(k)}^{(r)}\otimes\boldsymbol{\mu}_{(k)}^{(r)}\quad\text{and}\quad\mathbf{e}^{(r)}=\sum_{k=1}^{K}e_{(k)}^{(r)}\boldsymbol{\mu}_{(k)}^{(r)}\quad(r=1,\ldots,N) \tag{16}$$

define the viscous-compliance and 'residual' strain-rate tensors at the grain level in terms of the corresponding slip-level quantities $\alpha_{(k)}^{(r)}$ and $e_{(k)}^{(r)}$, respectively. For the voided phase, $(\mathbf{M}^{(0)})^{-1}=\mathbf{0}$ and $\mathbf{e}^{(0)}=\mathbf{0}$.

The local potentials $u^{(r)}$ of the nonlinear polycrystal are then approximated in terms of the local potentials $u_{L}^{(r)}$ of the above-defined linear-comparison polycrystal,

and a suitable measure of the error, to obtain the following approximation for the effective potential of the nonlinear polycrystal:

$$\widetilde{u}(\overline{\boldsymbol{\sigma}}) = (1-f)\sum_{r=1}^{N}\sum_{k=1}^{K} c_g^{(r)}\left[\phi_{(k)}^{(r)}(\hat{\tau}_{(k)}^{(r)}) - \phi_{(k)}^{(r)\prime}(\overline{\tau}_{(k)}^{(r)})\left(\hat{\tau}_{(k)}^{(r)} - \overline{\tau}_{(k)}^{(r)}\right)\right]. \tag{17}$$

In this expression, the variables $\hat{\tau}_{(k)}^{(r)}$ and $\overline{\tau}_{(k)}^{(r)}$ depend on the averages and fluctuations of the resolved shear stresses $\boldsymbol{\sigma}\cdot\boldsymbol{\mu}_{(k)}^{(r)}$ in the linear-comparison polycrystal defined by relations (6)–(16), subjected to a macroscopic stress $\overline{\boldsymbol{\sigma}}$. They are such that:

$$\overline{\tau}_{(k)}^{(r)} = \left\langle \boldsymbol{\sigma}\cdot\boldsymbol{\mu}_{(k)}^{(r)}\right\rangle^{(r)} = \overline{\boldsymbol{\sigma}}^{(r)}\cdot\boldsymbol{\mu}_{(k)}^{(r)} \tag{18}$$

and

$$\left(\hat{\tau}_{(k)}^{(r)} - \overline{\tau}_{(k)}^{(r)}\right)^2 = \left\langle\left(\boldsymbol{\sigma}\cdot\boldsymbol{\mu}_{(k)}^{(r)} - \overline{\tau}_{(k)}^{(r)}\right)^2\right\rangle^{(r)} = \boldsymbol{\mu}_{(k)}^{(r)}\cdot\mathbf{C}_{\boldsymbol{\sigma}}^{(r)}\boldsymbol{\mu}_{(k)}^{(r)}, \tag{19}$$

where the quantities $\hat{\tau}_{(k)}^{(r)} - \overline{\tau}_{(k)}^{(r)}$ are taken to have the same sign as the $\overline{\tau}_{(k)}^{(r)}$. Self-consistent estimates for the tensors $\overline{\boldsymbol{\sigma}}^{(r)}$ and $\mathbf{C}_{\boldsymbol{\sigma}}^{(r)}$ in terms of the local properties $\mathbf{M}^{(r)}$ and $\mathbf{e}^{(r)}$ are given by expressions (14) and (15) of Section 3.1.

In turn, the properties of the linear-comparison polycrystal must be specified such that the variables $e_{(k)}^{(r)}$ and $\alpha_{(k)}^{(r)}$ in relations (16) satisfy the relations

$$e_{(k)}^{(r)} = \phi_{(k)}^{(r)\prime}(\overline{\tau}_{(k)}^{(r)}) - \alpha_{(k)}^{(r)}\overline{\tau}_{(k)}^{(r)} \tag{20}$$

and

$$\phi_{(k)}^{(r)\prime}(\hat{\tau}_{(k)}^{(r)}) - \phi_{(k)}^{(r)\prime}(\overline{\tau}_{(k)}^{(r)}) = \alpha_{(k)}^{(r)}(\hat{\tau}_{(k)}^{(r)} - \overline{\tau}_{(k)}^{(r)}). \tag{21}$$

Note that relation (21) identifies the viscous slip compliances $\alpha_{(k)}^{(r)}$ of the linear-comparison polycrystal with a 'generalized-secant' approximation of the nonlinear constitutive relation for the corresponding slip systems in the viscoplastic polycrystal, taking into account both the average and fluctuation of the stress for the given grain orientation – as determined by the linear-comparison approximation, see Figure 1. Expressions (18)–(21) together with (14) constitute a system of nonlinear *algebraic* equations for the variables $\hat{\tau}_{(k)}^{(r)}$, $\overline{\tau}_{(k)}^{(r)}$ and $\alpha_{(k)}^{(r)}$, which must be solved numerically, in general. The solution of these equations and the 'generalized-secant' linearization scheme were implemented in the 'VPSC' (ViscoPlastic Self-Consistent) code, suitably modified to account for the presence of a compressible voided phase. Details of the algorithm can be found in [54].

Finally, an estimate for the effective behavior of the polycrystal can be obtained by differentiating (17) with respect to $\overline{\boldsymbol{\sigma}}$. It is given by

$$\overline{\boldsymbol{D}} = \overline{\boldsymbol{D}}_L - (1-f)\sum_{r=1}^{N}\sum_{k=1}^{K} c_g^{(r)}\left[(\phi_{(k)}^{(r)})''(\overline{\tau}_{(k)}^{(r)}) - \alpha_{(k)}^{(r)}\right]\left(\hat{\tau}_{(k)}^{(r)} - \overline{\tau}_{(k)}^{(r)}\right)\frac{\partial\overline{\tau}_{(k)}^{(r)}}{\partial\overline{\boldsymbol{\sigma}}}, \tag{22}$$

where $\overline{\boldsymbol{D}}_L$ is the macroscopic strain rate in the LCP, which is given in terms of the linear properties (16) by an expression of the form (13), and can be shown to reduce to

$$\overline{\boldsymbol{D}}_L = (1-f)\sum_{r=1}^{N}\sum_{k=1}^{K} c_g^{(r)}\phi_{(k)}^{(r)\prime}(\overline{\tau}_{(k)}^{(r)})\boldsymbol{\mu}_{(k)}^{(r)} + f(\widetilde{\mathbf{M}}+\widetilde{\mathbf{M}}^*)\overline{\boldsymbol{\sigma}}. \tag{23}$$

It is noted that the resulting stress–strain-rate relation (22) does not coincide exactly with the effective stress–strain-rate relation for the underlying linear-comparison polycrystal. It contains additional terms that depend on the derivatives of the average shear stresses $\overline{\tau}_{(k)}^{(r)}$, which must be determined by differentiating the system of Equations (18)–(21). An *alternative* approach for the estimation of the stress–strain-rate relation consists in the direct use of the effective stress–strain-rate relation (23) for the linear-comparison polycrystal. While this avoids the need to compute the derivatives of the quantities $\overline{\tau}_{(k)}^{(r)}$, however, it should be emphasized that the relation (23) does not possess an associated potential function $\widetilde{u}$ and is not exact to second-order in the heterogeneity contrast. It can be interpreted as a generalization of the so-called 'affine' approximation of Masson et al. [26], including the effect of field fluctuations (see [41] for more details).

3.3. *Nonlinear 'secant' estimates*

A simpler variational theory for nonlinear polycrystals is available from the work of deBotton and Ponte Castañeda [28]. This 'secant' theory, originally derived for the case of fully dense incompressible polycrystals, delivers rigorous bounds on the effective potential that can be used to assess the accuracy of other theories. In this section we extend it to account for the presence of a compressible voided phase.

The theory makes use of a linear-comparison voided polycrystal where the grain potentials are given by (6) with viscous compliances $\mathbf{M}^{(r)}$ given by $(16)_1$, but with strain-rate tensors $\mathbf{e}^{(r)}=\mathbf{0}$. For the voided phase, in turn, $(\mathbf{M}^{(0)})^{-1}=\mathbf{0}$ and $\mathbf{e}^{(0)}=\mathbf{0}$. The potentials $u^{(r)}$ of the nonlinear polycrystal are then approximated in terms of these linear potentials $u_L^{(r)}$ and a suitable measure of the error, to obtain the following approximation for the effective potential of the porous nonlinear polycrystal:

$$\widetilde{u}(\overline{\boldsymbol{\sigma}}) = (1-f)\sum_{r=1}^{N}\sum_{k=1}^{K} c_g^{(r)}\phi_{(k)}^{(r)}(\hat{\tau}_{(k)}^{(r)}). \tag{24}$$

The variables $\hat{\tau}_{(k)}^{(r)}$ in this expression depend on the resolved shear stresses $\boldsymbol{\sigma}\cdot\boldsymbol{\mu}_{(k)}^{(r)}$ in the linear-comparison polycrystal. They are such that

$$(\hat{\tau}_{(k)}^{(r)})^2 = \left\langle\left(\boldsymbol{\sigma}\cdot\boldsymbol{\mu}_{(k)}^{(r)}\right)^2\right\rangle^{(r)} = \boldsymbol{\mu}_{(k)}^{(r)}\cdot\langle\boldsymbol{\sigma}\otimes\boldsymbol{\sigma}\rangle^{(r)}\boldsymbol{\mu}_{(k)}^{(r)}. \tag{25}$$

Self-consistent estimates for the second moments $\langle\boldsymbol{\sigma}\otimes\boldsymbol{\sigma}\rangle^{(r)}$ in terms of the local properties $\mathbf{M}^{(r)}$ are given by expressions (14) of Section 3.1, with the $\mathbf{e}^{(r)}=\mathbf{0}$.

In turn, the properties of the linear-comparison polycrystal must be specified such that the variables $\alpha_{(k)}^{(r)}$ satisfy the relations

$$\phi_{(k)}^{(r)\prime}(\hat{\tau}_{(k)}^{(r)}) = \alpha_{(k)}^{(r)}\hat{\tau}_{(k)}^{(r)}. \tag{26}$$

Note that relation (26) identifies the viscous slip compliances $\alpha_{(k)}^{(r)}$ of the linear-comparison polycrystal with a 'secant' approximation of the nonlinear constitutive relation for the corresponding slip systems in the viscoplastic polycrystal, taking into account the second moments of the stress for the given grain orientation – as determined by the linear-comparison approximation, see Figure 1. Expressions (25)–(26) together with (14) constitute a system of nonlinear *algebraic* equations for the variables $\hat{\tau}_{(k)}^{(r)}$ and $\alpha_{(k)}^{(r)}$, which must be solved numerically, in general. Once again, the resolution of the above equations was implemented in the 'VPSC' code [54] by making use of the 'second-order' option and setting the eigenstrain-rates equal to zero. The variational 'secant' estimate (24) in fact provides a rigorous lower bound for all other estimates for $\widetilde{u}$ of the self-consistent type, and in particular, for the 'generalized-secant' estimates proposed above.

The effective behavior of the polycrystal follows from differentiation of (17) with respect to $\overline{\boldsymbol{\sigma}}$. It is given by

$$\overline{\boldsymbol{D}} = \overline{\boldsymbol{D}}_L = \widetilde{\mathbf{M}}\overline{\boldsymbol{\sigma}}. \tag{27}$$

Thus, unlike the 'generalized-secant' estimates, the 'secant' estimates for the stress–strain-rate relation coincide exactly with that of the underlying linear-comparison polycrystal. It is emphasized, however, that this stress–strain-rate relation is nonlinear, as it should be, since the slip-compliances $\alpha_k^{(r)}$, and therefore $\widetilde{\mathbf{M}}$, depend on $\overline{\boldsymbol{\sigma}}$.

4. Full-field simulations based on a fast Fourier transform algorithm

This numerical formulation is based on the fact that the local mechanical response of a heterogeneous medium can be calculated as a convolution integral between Green functions associated with appropriate fields in a linear reference homogeneous medium and the actual polarization (heterogeneity) field. A well-known technique, frequently used in combination with the Green function method, is to utilize Fourier transforms to reduce the convolution integrals in real space to simple products in Fourier space. For periodic microstructures, the FFT algorithm can be applied to transform the heterogeneity field into Fourier space and, in turn, get the mechanical fields by transforming the product of the latter with the Fourier transform of the Green function back to real space. However, since the actual polarization field depends precisely on the *a priori* unknown mechanical field, an iterative scheme has to be implemented to obtain, upon convergence, a compatible strain-rate field and a stress field in equilibrium.

In what follows, we describe the specialization of the FFT-based method to the case of viscoplasticity of polycrystals with voids. Moreover, since one of our goals is to assess the effect of crystallinity on the dilatational viscoplastic behavior of porous

materials, we will also address the FFT-based solution for voided materials with a nonlinear isotropic matrix.

4.1. *Unit cell construction*

The granular microstructures considered here are periodic unit cells generated by Voronoi tessellation, with intergranular cavities. The FFT-based calculation requires a discrete description of a unit cell on a regularly-spaced grid. Therefore, the generation procedure is simpler than in the case of having to determine the exact position of the boundaries between Voronoi cells and cavities in a continuum. We have proceeded as follows:

(1) N points were randomly distributed in a cubic domain (unit cell), and, to ensure periodicity of the microstructure, they were periodically duplicated immediately outside the unit cube. This Poisson distribution of points constituted the nuclei of the random grains. The results to be presented in Section 5 for untextured and textured specimens make use of $N = 200$ and $N = 1000$, respectively.
(2) The sides of the unit cell were partitioned into 128 points, determining a $128 \times 128 \times 128$ regular Fourier grid.
(3) Each Fourier point was assigned to its nearest nucleus (including those that were across the unit cell limits) determining N different domains (grains); see Figure 2a (case $N = 200$).
(4) All the identified Fourier points at multiple junctions were picked in a random sequence to try to accommodate a cavity of a radius r_1 (e.g. in the 5% porosity cases that follow, r_1 was chosen to be six times the distance between adjacent Fourier points) and surrounded by an 'exclusion' zone of radius r_2 ($> r_1$) where no other cavity was allowed (e.g. for 5% porosity, r_2 was set to nine times the distance between adjacent Fourier points).
(5) The above random process was stopped when the target overall porosity was reached, e.g. 5% for the microstructures analyzed in Section 5, see Figure 2b (and also 15%, as needed for the analysis of the effect of overall porosity, see Figures 6 and 10 below).

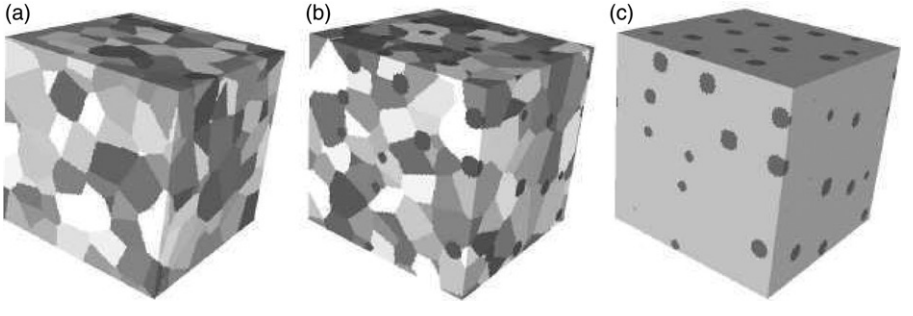

Figure 2. Unit cells used in FFT simulations: (a) fully dense polycrystal (200 grains); (b) voided polycrystal; (c) isotropic voided solid.

4.2. *Green's function method*

The discretization of the above periodic unit cell representing a porous polycrystal into $128 \times 128 \times 128$ Fourier points determines a regular grid in Cartesian space $\{\mathbf{x}^d\}$ and a corresponding grid of the same size in Fourier space $\{\boldsymbol{\xi}^d\}$. Either a velocity gradient $v_{i,j}$ (which can be decomposed into a symmetric strain-rate and an antisymmetric rotation rate: $\overline{v}_{i,j} = \overline{D}_{ij} + \overline{\Omega}_{ij}$) or a stress $\overline{\sigma}_{ij}$ is imposed on the unit cell. The local strain-rate field is a function of the local velocity field, i.e. $D_{ij}(v_k(\mathbf{x}))$, and can be split into its average and a fluctuation term: $D_{ij}(v_k(\mathbf{x})) = \overline{D}_{ij} + \tilde{D}_{ij}(\tilde{v}_k(\mathbf{x}))$, where $v_i(\mathbf{x}) = \overline{D}_{ij}x_j + \tilde{v}_i(\mathbf{x})$. Velocities and tractions along the boundary of the unit cell are to be determined. The velocity fluctuation field $\tilde{v}_i(\mathbf{x})$ is periodic across the boundary of the unit cell and the force field is antiperiodic.

The local constitutive relation between the strain-rate $D_{ij}(\mathbf{x})$ and the stress $\sigma_{ij}(\mathbf{x})$ for material points (i.e. belonging to grains) is given by (1) with (2) – note that the strain-rate has no dilatational component. As for the Fourier points belonging to voids, the stress vanishes and the strain-rate is non-traceless in general and needs to be determined. Let us choose a fourth-order tensor $\mathbf{L}^0$ to be the stiffness of a linear reference medium (the choice of $\mathbf{L}^0$ can be quite arbitrary, but the speed of convergence of the method will depend on this choice), and define the polarization field $\tau_{ij}(\mathbf{x})$ as

$$\boldsymbol{\tau}(\mathbf{x}) = \tilde{\boldsymbol{\sigma}}(\mathbf{x}) - \mathbf{L}^0\tilde{\boldsymbol{D}}(\mathbf{x}). \tag{28}$$

Then, the stress deviation can be written as

$$\tilde{\boldsymbol{\sigma}}(\mathbf{x}) = \mathbf{L}^0\tilde{\boldsymbol{D}}(\mathbf{x}) + \boldsymbol{\tau}(\mathbf{x}). \tag{29}$$

Combining Equation (29) with the equilibrium condition ($\sigma_{ij,j}(\mathbf{x}) = 0$) and the relation $\tilde{D}_{ij}(\mathbf{x}) = (\tilde{v}_{i,j}(\mathbf{x}) + \tilde{v}_{j,i}(\mathbf{x}))/2$, we obtain

$$L^0_{ijkl}\tilde{v}_{k,lj}(\mathbf{x}) + \tau_{ij,j}(\mathbf{x}) = 0. \tag{30}$$

The auxiliary system involving Green functions is then given by

$$L^0_{ijkl}G_{km,lj}(\mathbf{x} - \mathbf{x}') + \delta_{im}\delta(\mathbf{x} - \mathbf{x}') = 0. \tag{31}$$

After some manipulation, the convolution integral that gives the velocity-gradient deviation fields is

$$\tilde{v}_{i,j}(\mathbf{x}) = \int_{R^3} G_{ik,jl}(\mathbf{x} - \mathbf{x}')\tau_{kl}(\mathbf{x}')\mathrm{d}\mathbf{x}'. \tag{32}$$

Convolution integrals in direct space are simply products in Fourier space, hence

$$\hat{\tilde{v}}_{i,j}(\boldsymbol{\xi}) = \hat{\Gamma}_{ijkl}(\boldsymbol{\xi})\hat{\tau}_{kl}(\boldsymbol{\xi}), \tag{33}$$

where the symbol $\hat{}$ indicated a Fourier transform. The Green operator is defined as $\Gamma_{ijkl} = G_{ik,jl}$. The tensors $\hat{G}_{ij}(\boldsymbol{\xi})$ and $\hat{\Gamma}_{ijkl}(\boldsymbol{\xi})$ can be calculated by taking the Fourier transform of system (31):

$$\xi_i\xi_j L^0_{ijkl}\hat{G}_{km}(\boldsymbol{\xi}) = \delta_{im} \tag{34}$$

from where, defining the matrix $A_{ik}(\boldsymbol{\xi}) = L^0_{ijkl}\xi_j\xi_l$, we have

$$\hat{G}_{ij}(\boldsymbol{\xi}) = A^{-1}_{ij}(\boldsymbol{\xi}) \tag{35}$$

and

$$\hat{\Gamma}_{ijkl}(\boldsymbol{\xi}) = -\xi_j\xi_l\hat{G}_{ik}(\boldsymbol{\xi}). \tag{36}$$

4.3. *FFT-based algorithm*

The following iterative procedure is based on the augmented Lagrangians algorithm [47] adapted to the case of porous polycrystals, for a stress state imposed on the unit cell [55]. Supraindices indicate values corresponding to the current iteration (e.g. supraindex zero indicates the initial guess). The algorithm needs an initial guess for the average strain-rate, i.e. $\overline{D}^0_{ij} = \overline{D}'^0_{ij} + (\overline{D}^0_{kk}/3)\delta_{ij}$, which will be adjusted iteratively. Initial guess values also need to be assigned to the strain-rate field in the regular grid $\{\mathbf{x}^d\}$:

$$\tilde{D}'^0_{ij}(\mathbf{x}^d) = 0 \Rightarrow D'^0_{ij}(\mathbf{x}^d) = \overline{D}'_{ij} \quad \mathbf{x}^d \in \text{material and voids} \tag{37}$$

$$\tilde{D}^0_{kk}(\mathbf{x}^d) = -\overline{D}_{kk} \Rightarrow D^0_{kk}(\mathbf{x}^d) = 0 \quad \mathbf{x}^d \in \text{material} \tag{38}$$

$$\tilde{D}^0_{kk}(\mathbf{x}^d) = \frac{1-f}{f}\overline{D}_{kk} \quad \mathbf{x}^d \in \text{voids}. \tag{39}$$

With these initial values, the corresponding stress field $\boldsymbol{\sigma}^0(\mathbf{x}^d)$ at the crystalline material points is obtained by inverting the local constitutive relation, which requires us to know the initial values of the critical stresses $\tau^k_0(\mathbf{x}^d)$, and the Schmid tensors $\boldsymbol{\mu}_{(k)}(\mathbf{x}^d)$ (note that the hydrostatic component is zero). As for the points belonging to voids, simply, $\boldsymbol{\sigma}^0(\mathbf{x}^d) = \mathbf{0}$. The initial specification of these fields allows us to calculate the initial guess for the polarization field in direct space $\boldsymbol{\tau}^0(\mathbf{x}^d)$, which in turn can be Fourier-transformed to obtain $\hat{\boldsymbol{\tau}}^0(\boldsymbol{\xi}^d)$. Furthermore, assuming $\boldsymbol{\lambda}^0(\mathbf{x}^d) = \boldsymbol{\sigma}^0(\mathbf{x}^d)$ as the initial guess for a field of Lagrange multipliers associated with the compatibility constraints, the iterative procedure based on augmented Lagrangians proposed by Michel et al. [47] reads as follows. With the polarization field after iteration i being known, the $(i+1)$th iteration starts by computing the new guess for the kinematically-admissible strain-rate deviation field:

$$\hat{\tilde{\boldsymbol{d}}}^{i+1}(\boldsymbol{\xi}^d) = -\hat{\boldsymbol{\Gamma}}^{sym}(\boldsymbol{\xi}^d)\hat{\boldsymbol{\tau}}(\boldsymbol{\xi}^d), \quad \forall \boldsymbol{\xi}^d \neq \mathbf{0}, \quad \text{and} \quad \hat{\tilde{\boldsymbol{d}}}^{i+1}(\mathbf{0}) = \mathbf{0}, \tag{40}$$

where $\hat{\boldsymbol{\Gamma}}^{sym}$ is the Green operator, appropriately symmetrized. The corresponding field in real space is thus obtained by application of the inverse FFT, i.e.

$$\tilde{\boldsymbol{d}}^{i+1}(\mathbf{x}^d) = \text{fft}^{-1}\left\{\hat{\tilde{\boldsymbol{d}}}^{i+1}(\boldsymbol{\xi}^d)\right\} \tag{41}$$

and a new guess for the stress field in the grains is calculated from

$$\boldsymbol{\sigma}^{i+1}(\mathbf{x}^d) + \mathbf{L}^0\boldsymbol{D}^{i+1}(\mathbf{x}^d) = \boldsymbol{\lambda}^i(\mathbf{x}^d) + \mathbf{L}^0\left(\overline{\boldsymbol{D}}^i + \tilde{\boldsymbol{d}}^{i+1}(\mathbf{x}^d)\right), \tag{42}$$

which, using relation (1), leads to the following 6×6 system of nonlinear algebraic equations:

$$\boldsymbol{\sigma}^{i+1}(\mathbf{x}^d) + \mathbf{L}^0 \frac{\partial u}{\partial \boldsymbol{\sigma}}\left(\mathbf{x}^{\mathrm{d}}, \boldsymbol{\sigma}(\mathbf{x}^d)\right) = \boldsymbol{\lambda}^i(\mathbf{x}^d) + \mathbf{L}^0\left(\overline{\boldsymbol{D}}^i + \tilde{\boldsymbol{d}}^{i+1}(\mathbf{x}^d)\right). \tag{43}$$

The iteration is completed with the calculation of new guesses for the Lagrange multiplier field:

$$\boldsymbol{\lambda}^{i+1}(\mathbf{x}^d) = \boldsymbol{\lambda}^i(\mathbf{x}^d) + \mathbf{L}^0(\tilde{\boldsymbol{D}}^{i+1}(\mathbf{x}^d) - \tilde{\boldsymbol{d}}^{i+1}(\mathbf{x}^d)) \tag{44}$$

and the average strain-rate [55]:

$$\overline{\boldsymbol{D}}^{i+1} = \langle \boldsymbol{D}^i(\mathbf{x}^d)\rangle + (\mathbf{L}^0)^{-1}(\overline{\boldsymbol{\sigma}} - \langle \boldsymbol{\lambda}^{i+1}(\mathbf{x}^d)\rangle), \tag{45}$$

where $\langle\cdot\rangle$ indicates the average over the entire Fourier grid.

Note that Equations (42)–(44) are intended to enforce the convergence of: (a) $\boldsymbol{d}(\mathbf{x}^d)$ (i.e. the kinematically-admissible strain-rate field) towards $\boldsymbol{D}(\mathbf{x}^d)$ (i.e. the strain-rate field related to the stress through the constitutive equation) in fulfillment of compatibility, and (b) the Lagrange multiplier field $\boldsymbol{\lambda}(\mathbf{x}^d)$ towards the stress field $\boldsymbol{\sigma}(\mathbf{x}^d)$ to fulfill equilibrium. Once the values of the stress field have been determined, the local stress potential (1) can be calculated for every material point, and the effective stress potential is thus obtained as

$$\tilde{u}(\overline{\boldsymbol{\sigma}}) = (1-f)\left\langle u\left(\mathbf{x}^{\mathrm{d}}, \boldsymbol{\sigma}(\mathbf{x}^d)\right)\right\rangle_m, \tag{46}$$

where $\langle\cdot\rangle_m$ indicates the average over the material points.

5. Estimates for cubic and hexagonal power-law polycrystals

The methods presented above are used here to study the influence of crystallinity, texture and porosity on the instantaneous response of special – but representative – classes of porous polycrystalline solids. Of particular interest in this study is to assess the simplifying assumption made in essentially all homogenization-type theories of dilatational viscoplasticity that the matrix material surrounding the cavities is homogeneous and isotropic. For this reason, attention is restricted to polycrystalline solids with *isotropic* morphological statistics, that is, with 'equi-axed' grains and isotropically distributed porosity, but with possibly textured orientation distributions. In the linear-comparison theories of Section 3, these assumptions correspond to setting $\mathbf{Z} = \mathbf{I}$ in expression (11), but with possibly different weights $c_g^{(r)}$ for the various crystal orientations.

5.1. *Single-crystal behavior*

The single-crystal behavior is characterized by slip potentials of the common power-law form

$$\phi_{(k)}(\tau) = \frac{\tau_0^{(k)}\dot{\gamma}_0}{n+1}\left|\frac{\tau}{\tau_0^{(k)}}\right|^{n+1} \tag{47}$$

for *all* grains. Here, $m = 1/n$ ($0 \le m \le 1$) is the strain-rate sensitivity, $\dot{\gamma}_0$ is a reference strain rate, and $\tau_0^{(k)} > 0$ is the flow stress of the kth slip system in the 'reference' crystal. This class of slip potentials is particularly appropriate for investigating the effect of nonlinearity and grain anisotropy in a wide range of material behaviors. In particular, the limiting cases $m = 1$ and $m = 0$ correspond to linearly viscous and rigid-ideally plastic behaviors, respectively.

Two types of single-crystal anisotropy are considered:

(1) The first type corresponds to *high*-symmetry face-centered cubic (FCC) crystals that deform plastically through slip on a set of four slip planes of the type $\{111\}$ along three slip directions (per plane) of type $\langle 110\rangle$, which, together, constitute a set of 12 slip systems with suitably defined Schmid tensors $\boldsymbol{\mu}_{(k)}^{(r)}$. Of these, five are linearly independent, allowing arbitrary plastic deformation for the grains. For simplicity, all systems are assumed to have identical slip flow stresses $\tau_0^{(k)} = \tau_0$ for all $k = 1, \ldots, 12$.

(2) The second type corresponds to *low*-symmetry hexagonal closed-packed (HCP) crystals with ideal c/a ratio of 1.633, which are taken to deform plastically through two sets of slip systems: three prismatic systems ($\{10\bar{1}0\}\langle 11\bar{2}0\rangle$) and 12 first-order pyramidal-$\langle c+a\rangle$ slip ($\{10\bar{1}\bar{1}\}\langle 11\bar{2}\bar{3}\rangle$). Of these systems, five are linearly independent, allowing arbitrary plastic deformation for the grains. We take all prismatic systems to have slip flow stresses $\tau_0^{(k)} = \tau_A$, and all pyramidal systems to have slip flow stresses $\tau_0^{(k)} = \tau_B$, such that the ratio $M \doteq \tau_B/\tau_A = 5$.

5.2. *Polycrystal behavior and gauge surfaces*

Results are given below for untextured and textured polycrystals with a relatively large porosity level ($f = 0.05$) and two values of the viscous exponent n corresponding to linear ($n = 1$) and strongly nonlinear ($n = 10$) behaviors. In spite of the fact that the value $n = 1$ is unrealistic for most materials, the results are useful to assess the role of nonlinearity on the various findings since, as we have seen, the effective behavior of linear polycrystals is used to estimate the behavior of the nonlinear polycrystals.

The fact that the viscous exponent n and the reference strain rate $\dot{\gamma}_0$ are the same for all the slip systems and grains in a given polycrystal simplifies the analysis considerably. The local potential u is in this case a homogeneous function of degree $n+1$ in $\boldsymbol{\sigma}$, and consequently, the corresponding effective potential $\widetilde{u}$ is a homogeneous function of degree $n+1$ in $\overline{\boldsymbol{\sigma}}$ [31]. Then, a single equipotential surface $\widetilde{u}(\overline{\boldsymbol{\sigma}}) =$ constant in $\overline{\boldsymbol{\sigma}}$-space fully characterizes $\widetilde{u}$; any other equipotential surface is simply a homothetic surface [9]. Results for power-law polycrystals are reported here in the form of equipotential surfaces given by

$$\left\{\overline{\boldsymbol{\Sigma}} :\ \widetilde{u}(\overline{\boldsymbol{\Sigma}}) = \frac{\sigma_0^{-n}\dot{\gamma}_0}{n+1}\right\}, \tag{48}$$

where σ_0 is some reference flow stress – see below. This is the so-called *gauge surface* of the polycrystal, which characterizes completely the effective response [9]. The 'normal' to this surface in $\overline{\boldsymbol{\sigma}}$-space dictates the direction of macroscopic plastic flow in $\overline{\boldsymbol{D}}$-space. In the ideally-plastic limit, the gauge surface reduces to the yield surface

of the aggregate. The fact that $\widetilde{u}(\overline{\boldsymbol{\sigma}}) = \widetilde{u}(-\overline{\boldsymbol{\sigma}})$ implies point symmetry of the gauge surface about the origin, and (strict) convexity of $\widetilde{u}$ implies (strict) convexity of the gauge surface. Also note that a lower bound on $\widetilde{u}(\overline{\boldsymbol{\sigma}})$ translates into an outer bound on the gauge surface.

A more convenient equation for the gauge surface can be obtained by writing the function $\widetilde{u}$ as [9]

$$\widetilde{u}(\overline{\boldsymbol{\sigma}}) = \frac{\sigma_0 \dot{\gamma}_0}{n+1} \left(\frac{\Lambda(\overline{\boldsymbol{\sigma}})}{\sigma_0} \right)^{n+1}, \tag{49}$$

where the so-called *gauge factor* $\Lambda(\overline{\boldsymbol{\sigma}})$ is a homogeneous function of degree 1 in $\overline{\boldsymbol{\sigma}}$, which depends on the microstructure of the aggregate and on the material parameters n and $\tau_0^{(k)}$, but is independent of $\dot{\gamma}_0$. Then, the tensor

$$\overline{\boldsymbol{\Sigma}} = \frac{\overline{\boldsymbol{\sigma}}}{\Lambda(\overline{\boldsymbol{\sigma}})} \tag{50}$$

lies on the gauge surface (48). Thus, we can determine the gauge surface by computing the effective stress potential for macroscopic stresses $\overline{\boldsymbol{\sigma}}$ of arbitrary magnitude, determining the corresponding gauge factor from (49), and rescaling $\overline{\boldsymbol{\sigma}}$ according to (50).

With the objective of comparing predictions for the various material systems considered, we will report gauge surfaces for FCC and HCP *voided* polycrystals with σ_0 being the flow stress of the corresponding *fully dense* polycrystal with *isotropic* crystallographic and morphological textures. Recall that the flow stress $\widetilde{\sigma}_0$ of a fully dense isotropic polycrystal is defined by the identity (e.g. [31])

$$\widetilde{u}(\overline{\boldsymbol{\sigma}}) = \frac{\widetilde{\sigma}_0(\overline{\theta})\dot{\gamma}_0}{n+1} \left(\frac{\overline{\sigma}_e}{\widetilde{\sigma}_0(\overline{\theta})} \right)^{n+1}, \tag{51}$$

where $\overline{\sigma}_e = \sqrt{(3/2)\overline{\boldsymbol{\sigma}}' \cdot \overline{\boldsymbol{\sigma}}'}$ is the von Mises equivalent stress, and $\overline{\theta}$ is the Lode angle defined by $\cos(3\overline{\theta}) = (27/2)\det(\overline{\boldsymbol{\sigma}}'/\overline{\sigma}_e)$, with $\overline{\boldsymbol{\sigma}}'$ denoting the macroscopic stress deviator. Note that the effective flow stress is not a constant but actually depends on $\overline{\boldsymbol{\sigma}}'$ through the stress invariant $\overline{\theta}$. This stress invariant is homogeneous of degree zero in $\overline{\boldsymbol{\sigma}}'$, and characterizes the 'direction' of the applied stress in deviatoric space: the particular values $\overline{\theta} = 0$ and $\overline{\theta} = \pi/6$ correspond to axisymmetric shear and simple shear loadings, respectively. In the results reported below we set $\sigma_0 = \widetilde{\sigma}_0(0)$ and make use of the FFT method of Section 4 – with $f = 0$ – to compute it. The resulting values are given in Table 1.

Finally, we recall for later use that the overall stress triaxiality $\overline{X}_\sigma$ is defined as the ratio of the hydrostatic stress $\overline{\sigma}_m = (1/3)\mathrm{tr}\,\overline{\boldsymbol{\sigma}}$ to the von Mises equivalent stress $\overline{\sigma}_e$, and that uniaxial tension corresponds to $\overline{X}_\sigma = 1/3$. Corresponding invariants of $\overline{\boldsymbol{\Sigma}}$, denoted by $\overline{\Sigma}_m$ and $\overline{\Sigma}_e$, are defined similarly.

5.3. *The effect of crystallinity and porosity on the effective response*

We shall investigate first the effect of crystallinity and porosity on the effective response of untextured polycrystals. For conciseness, only axisymmetric loadings

Table 1. FFT estimates for the effective flow stress $\widetilde{\sigma}_0$ of fully dense polycrystals with FCC and HCP crystals, subjected to axisymmetric shear ($\overline{\theta} = 0$). The values are averages over three sets of results obtained by loading each specimen along three mutually orthogonal axes.

FCC – $\widetilde{\sigma}_0(0)/\tau_0$		HCP – $\widetilde{\sigma}_0(0)/\tau_A$	
$n=1$	$n=10$	$n=1$	$n=10$
1.499	2.574	3.627	7.733

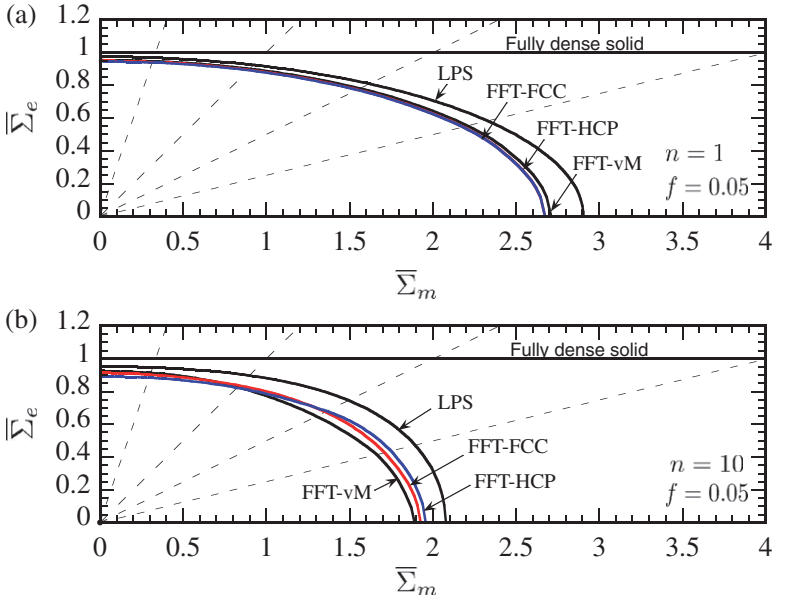

Figure 3. Gauge surfaces from FFT full-field simulations of untextured FCC and HCP polycrystalline solids and of a von Mises solid (vM) with porosity level $f = 0.05$ and viscous exponents (a) $n = 1$ and (b) $n = 10$. Also included are predictions of the viscoplastic Gurson-type model of Leblond, Perrin and Suquet (LPS) [9]. Dashed lines indicate directions of constant stress triaxialities $\overline{X}_\sigma = 1/3, 1, 2, 4$. Axisymmetric loadings ($\overline{\theta} = 0$).

with positive triaxialities are considered; other loadings lead to similar conclusions on the instantaneous response.

Figure 3 shows gauge surfaces, as defined by (48), calculated from FFT full-field simulations. Two hundred ($N = 200$) crystal orientations in the unit cell were prescribed according to a Sobol sequence [56] in order to generate polycrystalline voided solids with an effective response as close as possible to isotropy [57]. In this context, it should be noted that improved results could be generated, at least in principle, by considering ensemble averages of a sufficiently large number of realizations. However, in this work we will be satisfied with a the use of a 'representative' realization of the material for the purpose of making comparisons

with the corresponding homogenization estimates. For a given triaxiality, each specimen was loaded along three mutually orthogonal axes – amounting to actually considering three different, although not independent, realizations – and the effective stress potential was taken to be the average value. Also included for comparison purposes are gauge surfaces for von Mises (vM) voided solids. These surfaces were also obtained by the FFT method of Section 4, with the unit cell having the same distribution of cavities as those of the voided polycrystals – see Figure 2c – but with a von Mises isotropic response assigned to all Fourier points formerly belonging to 'grains'. The reference stress σ_0 in the vM gauge surfaces was identified with the flow stress of the von Mises matrix. In this representation, the gauge surface of a fully dense solid with either a polycrystalline or von Mises matrix is given by the line $\overline{\Sigma}_e = 1$, parallel to the hydrostatic axis.

We begin by noting that the FFT gauge surfaces are closed and convex as expected. The results show that the weakening effect due to the presence of cavities increases with increasing nonlinearity, cf. Figures 3a and b. Since the normal to the gauge surface dictates the direction of macroscopic flow, it follows that in a creep experiment under fixed stress triaxiality the nonlinear polycrystal will exhibit a larger hydrostatic strain rate than the linear polycrystal, and consequently, porosity will grow faster. The main observation in the context of this figure, however, is that crystallinity of the matrix material has a minor effect on the effective response within the entire range of nonlinearities considered. In the linear case, FCC and HCP surfaces are virtually indistinguishable from each other – see Figure 3a – while in the nonlinear case the surfaces remain very close to each other – see Figure 3b. Moreover, in both cases the von Mises surfaces lie very close to the polycrystal surfaces. Thus, the usual matrix isotropy assumption made in most available theories of dilatational viscoplasticity seems to be reasonable for *untextured* aggregates, even when the constituent crystals exhibit low symmetry. A generalization of Gurson's theory to von Mises voided solids exhibiting power-law viscoplasticity was proposed by Leblond, Perrin and Suquet [9]. Gauge surfaces predicted by this theory are shown in the figure – labeled LPS and given by expression (40) in that reference – and, indeed, fairly good agreement with FFT simulations is observed for both values of n – with the FFT results showing a somewhat softer response than the LPS model.

However small, the FFT simulations do show an influence of crystallinity on the effective response. In the linear case, the von Mises solid is always stronger than the polycrystalline solids – see Figure 3a – while in the nonlinear case, the von Mises solid is weaker than the polycrystalline solids under axisymmetric shear, but stronger under hydrostatic tension – see Figure 3b. This feature may be related to the role of crystal anisotropy on strain-rate localization. Figure 4 shows FFT maps of equivalent strain-rate, normalized by the macroscopic equivalent strain-rate, in polycrystalline (HCP and FCC) and von Mises voided solids under macroscopic stress triaxialities $\overline{X}_\sigma = 0, 6, \infty$ (note that, for a given triaxiality, the scales are identical for the three materials, but the maximum values of the strain-rate field strongly increase as triaxiality increases). At low triaxialities, the strain rate is mildly localized in bands inclined with respect the direction of the largest principal stress. In both the polycrystalline and von Mises solids, these localization bands are formed due to interaction between neighboring voids, but in the case of the polycrystalline solid the bands are more intense when traversing soft grains. Thus, crystallinity

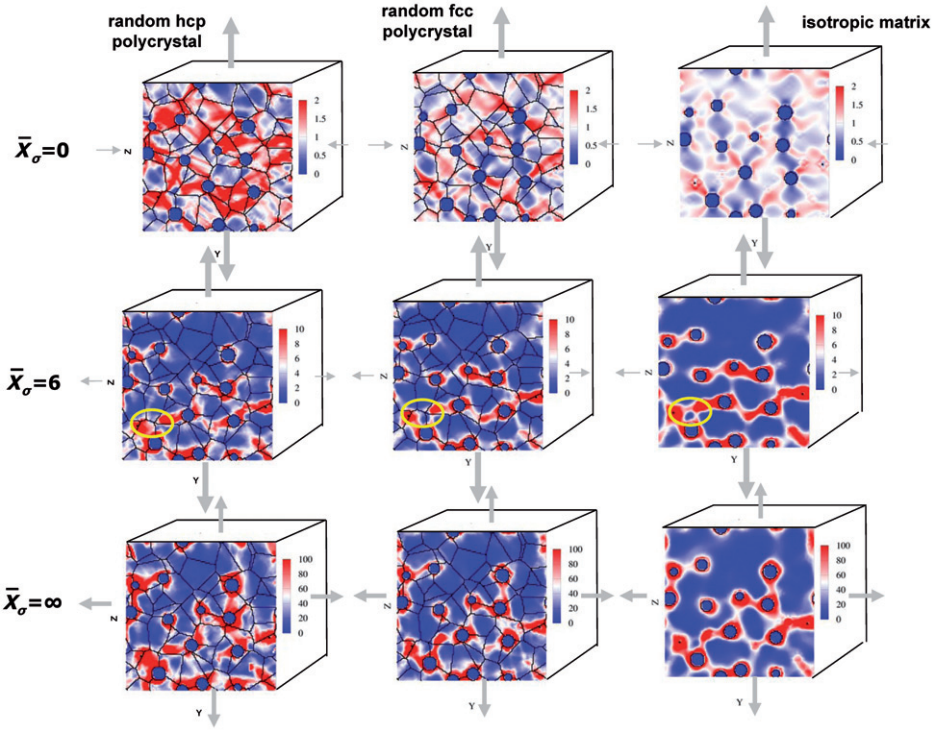

Figure 4. FFT maps of equivalent strain-rate (same 2-D section of the corresponding 3-D unit cells), normalized by the macroscopic equivalent strain-rate, in polycrystalline and von Mises voided solids under macroscopic stress triaxialities $\overline{X}_\sigma = 0, 6, \infty$. The porosity level is $f = 0.05$ and the viscous exponent is $n = 10$. The strain-rate is nullified inside the cavities to improve visualization of the field in the solid material.

seems to enhance localization at low triaxialities. As triaxiality increases, voids interact more strongly. In the case of large but finite triaxiality, the strongest localization bands are formed in regions that are normal to the direction of the largest principal stress. However, in the polycrystalline solid, some of these bands are disrupted by the presence of hard grains and grain boundaries – see the locations marked with yellow ellipses in the plots for $\overline{X}_\sigma = 6$, where the localization is appreciably lower in the polycrystal, compared with the same spot in the von Mises solid. Meanwhile, under purely hydrostatic tension, localization zones are stronger as the distance between interacting voids is smaller, irrespective of its orientation. In this case, disruptions of the localization zones related to crystallinity are harder to appreciate due to their very high intensity, but they can still be found.

Our interpretation of these differences is that, at low triaxialities, when the hydrostatic component of the strain-rate is small (or null) and the shear localization takes place mainly between voids that are close and favorably oriented with respect to each other (e.g. in the case of $\overline{X}_\sigma = 0$: at around 45° with respect to the axial direction), the (statistically) likely presence of at least one 'soft' crystal orientation (note that here and in what follows, 'soft' and 'hard' refer to the relative anisotropy

of the mechanical response with respect to the *local* states) linking well-oriented voids should increase the strain localization, determining an overall softer behavior, compared to an isotropic matrix material with the same distribution of voids. On the other hand, at high triaxialities, when the expansion of the voids has to accommodate the dilatation applied to the aggregate, so that the material that surrounds the cavities should undergo very large local (deviatoric) strains, the likely presence of at least one 'hard' grain in the voids' surroundings should disrupt the strain localization, leading to a harder response of the aggregate.

We now consider the different linear-comparison theories of Section 3. Figure 5 shows gauge surfaces predicted by the 'secant' (SEC) [28] and 'generalized-secant' (GSEC) [40] theories. In both cases, two hundred ($N=200$) equi-weighted grain orientations were prescribed according to a random process in order to generate polycrystalline voided solids with a fairly isotropic effective response. Also shown in this figure for comparison purposes are the 'affine' (AFF) linear-comparison estimates of the self-consistent type proposed in [26] and the FFT polycrystal results of Figure 3. For reasons that will become evident shortly, GSEC surfaces for $n=10$ have been plotted in continuous lines for $\overline{X}_\sigma \leq 2$ but in dotted lines for $\overline{X}_\sigma > 2$. We begin by noting that for $n=1$ all linear-comparison theories agree exactly with the linear self-consistent estimate on which they are based but give divergent predictions for $n=10$. Among the nonlinear theories, the GSEC estimates are seen to show the best overall performance. These estimates predict gauge surfaces that are closed,

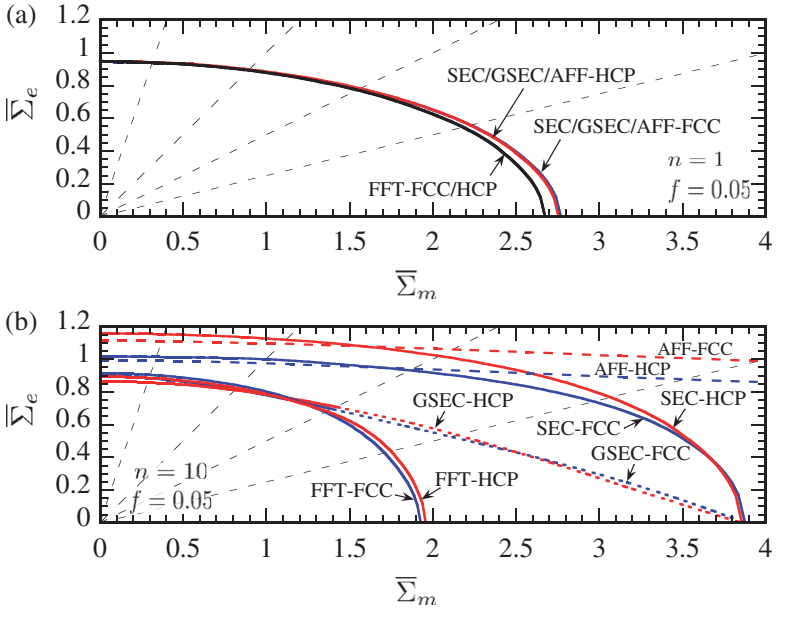

Figure 5. 'Secant' (SEC) [28] and 'generalized-secant' (GSEC) [40] estimates for the gauge surfaces of untextured FCC and HCP polycrystalline solids with porosity level $f=0.05$ and viscous exponents (a) $n=1$ and (b) $n=10$. FFT simulations are also shown for comparison purposes. Dashed lines indicate directions of constant stress triaxialities $\overline{X}_\sigma = 1/3, 1, 2, 4$. Axisymmetric loadings ($\overline{\theta}=0$).

convex, and that lie within the SEC surfaces, as they should. Recall that the SEC estimates are rigorous outer bounds for all other linear-comparison estimates of the self-consistent type, and in particular, for the GSEC estimates. More importantly, GSEC surfaces show the best agreement with FFT simulations. In particular, they agree with FFT simulations in that gauge surfaces of untextured polycrystals are fairly insensitive to matrix crystallinity within the entire range of nonlinearities considered. The SEC estimates, on the other hand, give stronger predictions – consistent with their outer bound character – and show a noticeable difference between FCC and HCP surfaces at low triaxialities. However, the performance of both GSEC and SEC models constitute a substantial improvement over that of classical polycrystalline models. The AFF model is representative of this class of models: it produces unphysical non-convex gauge surfaces with unbounded hydrostatic strength – see Figure 5b. This poor performance at large triaxialities is a direct consequence of a linearization scheme solely based on the first moments of the local fields. The secant and generalized-secant linearization schemes utilized in this work involve the second moments and as a consequence give superior predictions.

Now, while very accurate at low to moderate triaxialities, $0 \leq \overline{X}_\sigma \lesssim 2$, GSEC estimates are seen to give overly strong predictions at larger triaxialities. At the hydrostatic point, these estimates agree exactly with the SEC bound and are roughly twice as strong as the FFT results. Moreover, unlike the smooth FFT surfaces, they exhibit a corner at that point. As a result, GSEC predictions for highly triaxial creeping processes will give unrealistically small hydrostatic strain rates and consequently will underestimate void growth at the initial stages of deformation. This problem of variational linear-comparison estimates is already well known in the context of von Mises voided solids [58,59]. However, Danas et al. [60] have proposed an *ad hoc* remedy whereby the linearization scheme is forced to depend explicitly on the macroscopic stress triaxiality in such a way that the effective gauge surface tends to some specified hydrostatic point. In the case of von Mises solids, a suitable hydrostatic point is available from the well-known solution of a hollow shell. A similar strategy could be envisaged for voided polycrystalline solids and will be explored in future work; in this connection, the recent work of Idiart [61,62] for sequentially laminated composites could prove helpful. In any event, as it stands, the generalized-secant theory proposed in this work should be accurate enough to model deformation processes involving low to moderate stress triaxialities.

For completeness, trends as a function of porosity are explored in Figure 6. Since the linear-comparison theories derived in this work have been found to be inaccurate at large stress triaxialities, we shall restrict attention to the purely deviatoric response. GSEC predictions and FFT results are thus given in the form of $\overline{\Sigma}_e$ versus f for two values of the viscous exponent ($n = 1, 10$). Theoretical and numerical results show a fairly linear decrease of $\overline{\Sigma}_e$ with increasing f for both values of n and porosity levels of up to $f = 0.15$. The main observation, however, is that FFT results show that the influence of matrix crystallinity on the effective response remains relatively small at large porosity levels, even for the strongly nonlinear polycrystals. The GSEC estimates are in good agreement with the FFT results for $n = 1$, but exhibit a somewhat more pronounced influence of matrix crystallinity than the FFT results for $n = 10$. It should be noted, however, that porosity levels beyond 0.15 are hardly

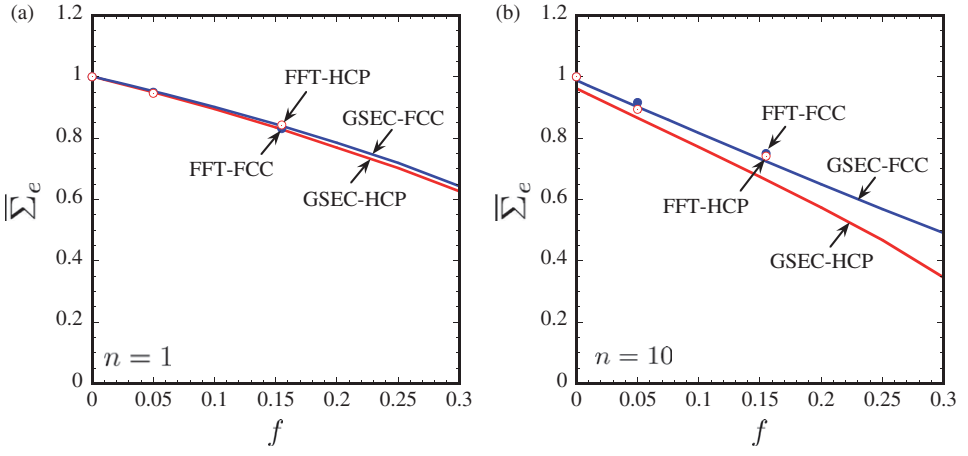

Figure 6. Deviatoric response of untextured voided polycrystals as a function of porosity f: (a) linear ($n = 1$) and (b) nonlinear ($n = 10$) polycrystals.

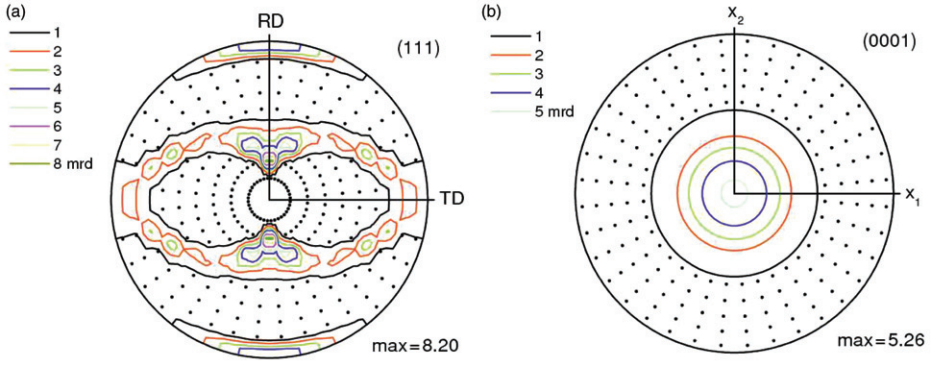

Figure 7. Crystallographic textures considered: (a) (111) pole figure of a rolled FCC polycrystal with normal direction (ND) in the center; (b) basal pole figure of an HCP polycrystal with axisymmetric texture and axial direction (x_3) in the center. Intensity lines correspond to multiples of random distribution (mrd). Dots correspond to regions of the pole figures with intensities lower than that of the random distribution (1 mrd).

met in practice and the dependence on matrix crystallinity exhibited by the nonlinear GSEC estimates remains relatively small when the porosity level is below that value.

5.4. *The effect of crystallographic texture and porosity on the effective response*

We now assess the effect of crystallographic texture and porosity on the effective response. Textures are simulated by a set of one thousand ($N = 1000$) crystal orientations: FCC polycrystals are given a sharp rolling texture represented by the (111) pole figure of Figure 7a, while HCP polycrystals are given a sharp transversely isotropic texture represented by the (0001) pole figure of Figure 7b.

In both cases, specimens are subjected to axisymmetric stress states with positive triaxiality and principal axes aligned with the symmetry axes of the microstructure. FCC specimens are loaded in axisymmetric tension along the rolling, normal and transverse directions, while HCP specimens are loaded along parallel and perpendicular directions to the axis of transverse isotropy. For a given orientation of the tensile axis, these axisymmetric stress states can be described by the von Mises and hydrostatic stress measures. Gauge surfaces obtained by FFT numerical simulations and generalized-secant estimates are given in Figures 8 and 9. Secant estimates are omitted in this section for ease of presentation. Also included in these figures for comparison purposes are the corresponding gauge surfaces for untextured specimens.

We begin by noting that all gauge surfaces are closed and convex, as expected. It is observed that numerical simulations and theoretical estimates both predict a minor influence of crystallographic texture on the effective response of polycrystalline solids when the crystal symmetry is high – see Figures 8a and b. On the other hand, when the crystal symmetry is low, corresponding to large grain anisotropy, the effective response is significantly influenced by texture, especially for low strain-rate sensitivity ($m = 1/n$) – see Figures 9a and b. In all cases, it is interesting to remark that the effect of grain anisotropy and texture on the flow stress under purely hydrostatic conditions is relatively minor. In view of these results, we conclude that the assumption of matrix isotropy is clearly inadequate for textured low-symmetry polycrystals, and polycrystalline models like the ones that we have developed in this

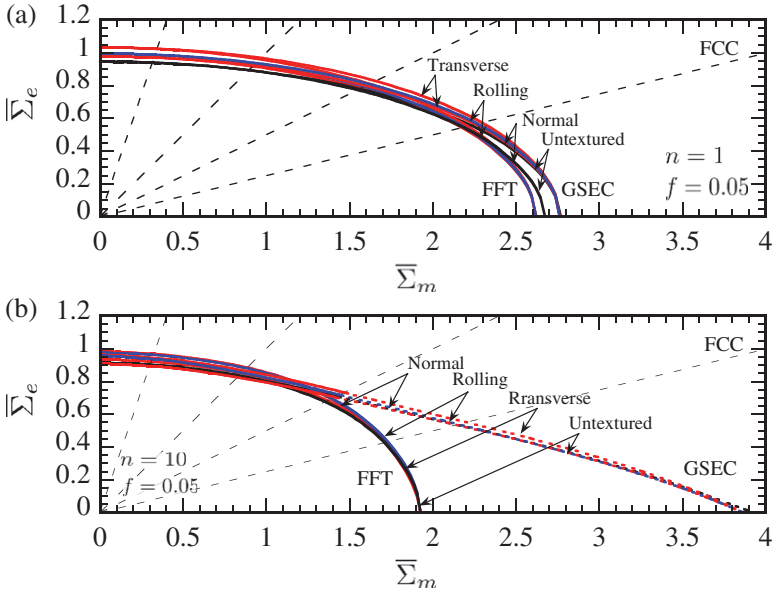

Figure 8. Gauge surfaces from FFT simulations and 'generalized-secant' (GSEC) theory [40] of a rolled FCC polycrystal under axisymmetric loadings with tensile axis along three different directions: rolling, normal, and transverse directions. The porosity level is $f = 0.05$ and the viscous exponents are (a) $n = 1$ and (b) $n = 10$. Dashed lines indicate directions of constant stress triaxialities $\overline{X}_\sigma = 1/3, 1, 2, 4$.

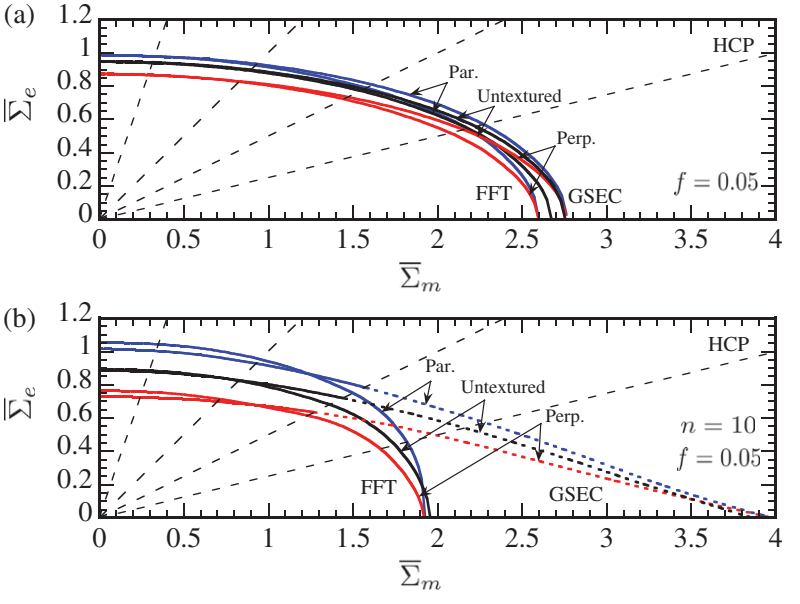

Figure 9. Gauge surfaces from FFT simulations and 'generalized-secant' (GSEC) theory [40] of an axisymmetrically textured HCP polycrystal with a strong basal component along the 'parallel' direction. The porosity level is $f = 0.05$ and the viscous exponents are (a) $n = 1$ and (b) $n = 10$. Dashed lines indicate directions of constant stress triaxialities $\overline{X}_\sigma = 1/3, 1, 2, 4$.

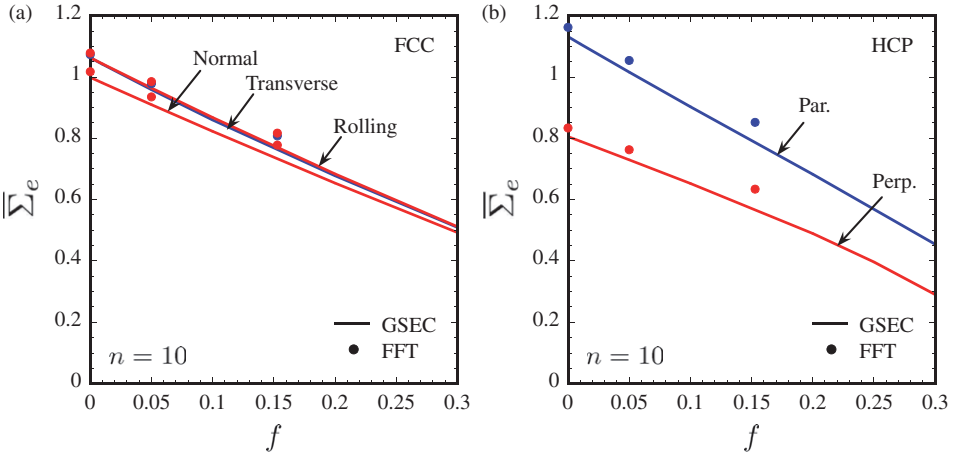

Figure 10. Deviatoric response of textured voided polycrystals as a function of porosity f: (a) FCC and (b) HCP polycrystals. The viscous exponent is $n = 10$.

work are required. In parallel with earlier observations for untextured polycrystals, it is noted that the GSEC estimates also predict closed and convex gauge surfaces, as they should, and exhibit good agreement with numerical simulations in general, but for $n = 10$ and large stress triaxialities ($\overline{X}_\sigma > 2$) they give overly strong predictions.

As mentioned above, however, these estimates already constitute a substantial improvement over earlier linear-comparison estimates.

Finally, trends as a function of porosity are explored in Figure 10. Once again, we restrict attention to the purely deviatoric response. GSEC predictions and FFT results are given in the form of $\overline{\Sigma}_e$ versus f for the FCC and HCP textured polycrystals with $n = 10$. As already observed in untextured polycrystals, theoretical and numerical results show a fairly linear decrease of $\overline{\Sigma}_e$ with increasing f for porosity levels of up to $f = 0.15$. The main observation, however, is that FFT results and GSEC predictions show that the influence of matrix crystallinity and crystallographic texture on the effective response already found for $f = 0.05$ persists for the entire range of porosities considered.

6. Summary and concluding remarks

We have carried out numerical simulations and theoretical calculations for the viscoplasticity of polycrystalline solids containing intergranular cavities. The simulations followed from a fast Fourier transform algorithm originally developed by Moulinec and Suquet [45,46]. The theoretical predictions, in turn, were obtained by means of suitable extensions of the variational linear-comparison theories of deBotton and Ponte Castañeda [28] and Liu and Ponte Castañeda [40] for porous polycrystals.

The simultaneous effects of porosity, crystallinity and crystallographic texture were investigated in both linear and strongly nonlinear solids. Numerical simulations and theoretical predictions both indicate that the *effective response* of untextured voided solids is relatively insensitive to the crystallinity of the polycrystalline matrix, even when crystal symmetry and strain-rate sensitivity are low. By contrast, the effective response of strongly textured voided solids was found to be quite sensitive to matrix crystallinity when crystal symmetry and strain-rate sensitivity are both sufficiently low. In this case, standard models based on isotropic-matrix theories are inadequate and polycrystalline theories like the ones presented in this work should be employed. In this connection, it is emphasized that even if the crystal structure exhibits many geometrical symmetries (e.g. FCC and BCC crystals), local processes like strain hardening may introduce a strong anisotropy in the crystal's response upon large deformations, further restricting the range of validity of isotropic-matrix models.

Meanwhile, our findings at the *local level* seem to indicate that, at low triaxialities, the crystallinity of the matrix increases the strain localization due to the statistically likely presence of 'soft links' (i.e. at least one soft crystal) in the surroundings of interacting voids, while the opposite happens for high triaxialities, i.e. the likely presence of at least one 'hard' crystal in the vicinities of expanding cavities may disrupt strain localization.

Among the polycrystalline theories considered, the generalization of the secant second-order theory of Liu and Ponte Castañeda [40] was found to be the most accurate. Unlike classical theories, it correctly predicts closed and convex gauge surfaces and satisfies available bounds. Moreover, the predictions were in good agreement with the numerical simulations in general. With decreasing strain-rate

sensitivity, however, the predictions become progressively less accurate at large stress triaxialities ($\overline{X}_\sigma \gtrsim 2$). This is a well-known issue in variational linear-comparison theories, which will be addressed in future work. In this context, it is important to emphasize that this limitation of the variational linear-comparison methods for porous media has already been addressed successfully for isotropic-matrix materials [60], and it seems reasonable that improved models for porous materials with anisotropic (textured) polycrystalline solid phases may be possible following similar ideas. The key point is the generation of improved estimates for the hydrostatic point, which may be feasible by means of an appropriate generalization of the sequential lamination methods, which has been shown to recover the exact result at least for the isotropic-matrix case [62]. In any event, as it stands, the generalized-secant theory proposed in this work should be appropriate to model deformation processes involving stress triaxialities in the range $0 \leq \overline{X}_\sigma \lesssim 2$. While this may not be suitable for some applications, such as HIPing, it may provide useful approximations in other approximations with lower overall triaxialities.

The present work has demonstrated the capabilities of the FFT algorithm to model voided polycrystals. It is emphasized, however, that the reported results were based on a single unit-cell realization and therefore do not account for the expected statistical deviations due to microstructural randomness. More accurate results that do account for such deviations can be produced by ensemble averaging multiple realizations as in the work of Moulinec and Suquet [63] on two-phase composites.

This study has focused on the instantaneous viscoplastic response of polycrystalline voided solids. By integrating this response along with appropriate evolution laws for the various microstructural variables over time, as has already been done for isotropic-matrix porous materials [64,65], as well as for fully dense polycrystalline aggregates [40,43], a more general micromechanical theory of dilatational viscoplasticity accounting for the simultaneous evolution of texture and porosity can be achieved. This is in contrast to Gurson-type theories recently proposed in the literature [12–14], which rely on phenomenological descriptions of texture effects. Efforts to derive such micromechanical theories, and their corresponding numerical implementation, are currently under way and will be reported in due time.

Acknowledgements

The authors wish to thank Prof. Pierre Suquet (Laboratoire de Mécanique et d'Acoustique/CNRS, Marseille, France) for his many useful comments on this work. The work of RAL was supported by Joint DoD/DOE Munitions Technology Program and LANL LDRD-DR 2010026 Programs. The work of PPC was partially supported by Joint DoD/DOE Munitions Technology Program under LANL subcontract number 76847-001-09. PPC also acknowledges support from the National Science Foundation under grant CMMI-0654063.

References

[1] S. Caré and A. Zaoui, Acta Mater. 44 (1996) p.1323.
[2] L. Wayne, K. Krishnan, S. DiGiacomo, N. Kovvali, P. Peralta, S.N. Luo, S. Greenfield, D. Byler, D. Paisley, K.J. McCellan, A. Koskelo and R. Dickerson, Scripta Mater. 63 (2010) p.1065.

[3] M.R. Bache and W.J. Evans, Mater. Sci. Eng. A 319–321 (2001) p.409.
[4] R.A. Lebensohn, D. Solas, G. Canova and Y. Brechet, Acta Mater. 44 (1996) p.315.
[5] S.J. Hales and R.A. Hafley, Mater. Sci. Eng. A 257 (1998) p.153.
[6] G.T. Gray III, N.K. Bourne, M.A. Zocher, P.J. Maudlin and J.C.F. Millett, *Influence of crystallographic anisotropy on the Hopkinson fracture ''spallation'' of zirconium*, in *Shock Compression of Condensed Matter – 1999*, M.D. Furnish, L.C. Chhabildas and R.S. Hixson, eds., AIP Press, Woodbury, NY, 2000, p.509.
[7] J.C.F. Millett, G. Whiteman, N.K. Bourne and G.T. Gray III, J. Appl. Phys. 104 (2008) p.073531.
[8] A.L. Gurson, J. Eng. Mat. Tech. 99 (1977) p.2.
[9] J.-B. Leblond, G. Perrin and P. Suquet, Int. J. Plasticity 10 (1994) p.213.
[10] M. Gologanu, J.B. Leblond and J. Devaux, J. Mech. Phys. Solids 41 (1993) p.1723.
[11] M. Gărăjeu, J.C. Michel and P. Suquet, Comput. Meth. Appl. Mech. Eng. 183 (2000) p.223.
[12] A.A. Benzerga, J. Besson and A. Pineau, Acta Mater. 52 (2004) p.4639.
[13] V. Monchiet, O. Cazacu, E. Charkaluk and D. Kondo, Int. J. Plasticity 24 (2008) p.1158.
[14] S.M. Keralavarma and A.A. Benzerga, J. Mech. Phys. Solids 58 (2010) p.874.
[15] R. Hill, Proc. Roy. Soc. London A 193 (1948) p.281.
[16] R.A. Lebensohn, Y. Liu and P. Ponte Castañeda, Proc. Roy. Soc. Lond. A 460 (2004) p.1381.
[17] R.A. Lebensohn, Y. Liu and P. Ponte Castañeda, Acta Mater. 52 (2004) p.5347.
[18] A.V. Hershey, ASME J. Appl. Mech. 21 (1954) p.236.
[19] E. Kröner, Z. Phys. 151 (1958) p.504.
[20] Z. Hashin and S. Shtrikman, J. Mech. Phys. Solids 10 (1962) p.343.
[21] J.R. Willis, J. Mech. Phys. Solids 25 (1977) p.185.
[22] R. Hill, J. Mech. Phys. Solids 13 (1965) p.89.
[23] J.W. Hutchinson, Proc. Roy. Soc. London A 348 (1976) p.101.
[24] A. Molinari, G.R. Canova and S. Ahzi, Acta Metall. Mater. 35 (1987) p.2983.
[25] R.A. Lebensohn and C.N. Tomé, Acta Metall. Mater. 41 (1993) p.2611.
[26] R. Masson, M. Bornert, P. Suquet and A. Zaoui, J. Mech. Phys. Solids 48 (2000) p.1203.
[27] P. Ponte Castañeda and M. Nebozhyn, Proc. Roy. Soc. A 453 (1997) p.2715.
[28] G. deBotton and P. Ponte Castañeda, Proc. Roy. Soc. A 448 (1995) p.121.
[29] P. Ponte Castañeda, J. Mech. Phys. Solids 39 (1991) p.45.
[30] P. Suquet, C.R. Acad. Sci. Paris II 317 (1995) p.1515.
[31] P. Ponte Castañeda and P. Suquet, Adv. Appl. Mech. 34 (1998) p.171.
[32] M. Nebozhyn, P. Gilormini and P. Ponte Castañeda, C.R. Acad. Sci. Paris IIB. 328 (2000) p.11.
[33] M.I. Idiart and P. Ponte Castañeda, Proc. Roy. Soc. A 463 (2007) p.907.
[34] M.I. Idiart and P. Ponte Castañeda, Proc. Roy. Soc. A 463 (2007) p.925.
[35] M. Bornert, R. Masson, P. Ponte Castañeda and A. Zaoui, J. Mech. Phys. Solids 49 (2001) p.2737.
[36] P. Ponte Castañeda, J. Mech. Phys. Solids 44 (1996) p.827.
[37] P. Ponte Castañeda and J.R. Willis, Proc. Roy. Soc. A 455 (1999) p.1799.
[38] M.V. Nebozhyn and P. Ponte Castañeda, *Second-order estimates for the effective behavior of nonlinear porous materials*, in *IUTAM Symposium on Transformation Problems in Composite and Active Materials*, Y. Bahei-El-Din and G.J. Dvorak, eds., Kluwer Academic Publishers, New York, 1998, p.73.
[39] Y. Leroy and P. Ponte Castañeda, C.R. Acad. Sci. Paris IIB. 329 (2001) p.571.
[40] Y. Liu and P. Ponte Castañeda, J. Mech. Phys. Solids 52 (2004) p.467.
[41] P. Ponte Castañeda, J. Mech. Phys. Solids 50 (2002) p.737.
[42] Y. Liu, P. Gilormini and P. Ponte Castañeda, Tectonophys. 406 (2005) p.179.

[43] R.A. Lebensohn, C.N. Tomé and P. Ponte Castañeda, Phil. Mag. 87 (2007) p.4287.
[44] R.A. Lebensohn, C.N. Tomé and P.J. Maudlin, J. Mech. Phys. Solids 52 (2004) p.249.
[45] H. Moulinec and P. Suquet, C.R. Acad. Sci. Paris II 318 (1994) p.1417.
[46] H. Moulinec and P. Suquet, Comput. Meth. Appl. Mech. Eng. 157 (1998) p.69.
[47] J. Michel, H. Moulinec and P. Suquet, Comput. Model. Eng. Sci. 1 (2000) p.79.
[48] R.A. Lebensohn, Acta Mater. 49 (2001) p.2723.
[49] P. Ponte Castañeda, *Nonlinear composite materials: effective constitutive behavior and microstructure evolution*, in *Continuum Micromechanics*, CISM Courses and Lecture Notes, Vol. 377, P. Suquet, ed., Springer-Verlag, Wien, 1997, p.131.
[50] M.I. Idiart and P. Ponte Castañeda, Proc. Roy. Soc. A 463 (2007) p.183.
[51] N. Laws, J. Mech. Phys. Solids 21 (1973) p.9.
[52] J.R. Willis, Adv. Appl. Mech. 21 (1981) p.1.
[53] P.-G. Vincent, Y. Monerie and P. Suquet, C.R. Mécanique 336 (2008) p.245.
[54] C.N. Tomé and R.A. Lebensohn, Manual for Code Viscoplastic Self-Consistent (version 7). Available at http://public.lanl.gov/lebenso/vpscmanual.pdf.
[55] J. Michel, H. Moulinec and P. Suquet, Int. J. Numer. Meth. Eng. 52 (2001) p.139.
[56] I.M. Sobol, USSR Comput. Math. Math. Phys. 7 (1967) p.86.
[57] R. Brenner, R.A. Lebensohn and O. Castelnau, Int. J. Solids Struct. 46 (2009) p.3018.
[58] J. Pastor and P. Ponte Castañeda, C.R. Mécanique 330 (2002) p.741.
[59] N. Bilger, F. Auslender, M. Bornert and R. Masson, C.R. Mécanique 330 (2002) p.127.
[60] K. Danas, M.I. Idiart and P. Ponte Castañeda, Int. J. Solids Struct. 45 (2008) p.3392.
[61] M.I. Idiart, C.R. Mecanique 335 (2007) p.363.
[62] M.I. Idiart, J. Mech. Phys. Solids 56 (2008) p.2599.
[63] H. Moulinec and P. Suquet, *Homogenization for nonlinear composites in the light of numerical simulations*, in *Nonlinear Homogenization and Its Applications to Composites, Polycrystals and Smart Materials*, P. Ponte Castañeda, J.J. Telega and B. Gambin, eds., Kluwer Academic Publishers, Dordrecht, 2004, p.193.
[64] K. Danas and P. Ponte Castañeda, Eur. J. Mech. A Solids 28 (2009) p.387.
[65] K. Danas and P. Ponte Castañeda, Eur. J. Mech. A Solids 28 (2009) p.402.